INTERNATIONAL JOURNAL OF CLIMATOLOGY
Int. J. Climatol. (2014)
Published online in Wiley Online Library
(wileyonlinelibrary.com) DOI: 10.1002/joc.3912

Statistical relationship between remote climate indices and West African monsoon variability

Samo Diatta[a,b] and Andreas H. Fink[c]*
[a] *Laboratory for Oceanography, Environment and Climate Sciences, Ziguinchor, Senegal*
[b] *Laboratory for Atmospheric and Oceanic Physics, Dakar, Senegal*
[c] *Institute for Meteorology and Climate Research, Karlsruhe Institute for Technology, Karlsruhe, Germany*

ABSTRACT: This paper revisits the strength and stationarity of linear statistical relationships between indices of monsoon rainfall derived from rain gauge data for three regions in tropical West Africa [West Sahel (WS), Central Sahel (CS), and Guinea Coast (GC)] and various indices describing remote variations in the ocean–atmosphere climate systems from 1921 to 2009. The results reveal that both the Atlantic Multi-decadal Oscillation (AMO) and the Atlantic Meridional Mode (AMM) show a positive linear correlation to Sahel rainfall. The percent variance explained (PVE) ranges from 10 to 25%. The correlation stems from periods longer than 8 years for AMO, but AMM does show a correlation on interannual time scales for WS that was absent in the 1970s and 1980s. The PVE by El Niño Southern Oscillation (ENSO) indices is, though statistically significant, on the order of 10% and found mainly on the interannual time scale. A strong and stable correlation with PVEs larger than 50% is found between the sea surface temperatures (SSTs) in the Atlantic 3 region (ATL3, 0°–20°W, 3°S–3°N) and the GC rainfall. On the other hand, the correlation between ATL3 and WS rainfall changed from significantly negative to significantly positive after the 1970s. The Eastern Mediterranean SSTs are found to be significantly related to CS rainfall, especially in recent years with PVEs between 36 and 47%. Multi-linear regression analyses reveal that the relative importance of the Indian Ocean is 42% in the optimal regression model. For the CS, this value is 37% for the Eastern Mediterranean SSTs and 70% in case of the GC using the ATL3 index. However, except for the GC, non-stationarities in the correlation between the climate state indexes and West African monsoon (WAM) rainfall suggest the need of the application of different regression models depending on the active 'teleconnection regime'.

KEY WORDS West African monsoon; teleconnections; rainfall variability

Received 21 December 2012; Revised 23 November 2013; Accepted 4 December 2013

1. Introduction

The causes of variability of the West African monsoon (WAM) on different temporal and spatial scales remain a grand research challenge, with important ramifications to West African societies. On the continental scale, the WAM rainfall is influenced by remote variations of the atmosphere–ocean systems via so-called teleconnections. This knowledge emerged from numerous studies trying to explain the severe Sahel drought in the 1970s and 1980s. Several studies conclude from modelling approaches that in the 20th century, oceanic forcing was the dominant driver of Sahel rainfall variability on interannual and decadal time scales with vegetation changes likely enhancing the externally, sea surface temperature (SST)-induced signal (e.g. Rowell *et al.*, 1995; Zeng *et al.*, 1999; Biasutti *et al.*, 2008). Numerous observational and modelling studies have tried to attribute interannual to decadal SST anomaly patterns in global oceans, as well as in individual tropical ocean basins and the Mediterranean Sea to simultaneous or lagged responses in WAM rainfall.

Folland *et al.* (1986) and Hoerling *et al.* (2006), for example, attribute the decadal drying phase in the Sahel in 1970s to an inter-hemispheric temperature gradient in the global ocean basins with a particular strong signal in the Atlantic Ocean. As a consequence of the latter, these inter-hemispheric SST fluctuations are related to the Atlantic Multi-decadal Oscillation (AMO), a coherent pattern of the multi-decadal variability in SSTs centred on the North Atlantic Ocean (Kerr, 2000). The AMO has been linked to the occurrence of Sahel droughts (Sutton and Hodson, 2005) and the recent partial rainfall recovery in the Sahel (Hagos and Cook, 2008; Mohino *et al.*, 2011a). A north–south SST dipole, straddling the equator in the Atlantic Ocean, is known as the Atlantic Meridional Mode (AMM). Kossin and Vimont (2007) argue that the AMM is a physical coupled ocean–atmosphere mode whereas the AMO is a statistical mode. On multi-decadal time scales, AMM is likely to be excited by the AMO. They show that the AMM is more closely related to the Atlantic hurricane activity than AMO. At the same

* Correspondence to: A. H. Fink, Institute for Meteorology and Climate Research, Karlsruhe Institute for Technology, Wolfgang-Gaede-Weg 1, D-76131 Karlsruhe, Germany. E-mail: andreas.fink@kit.edu

time, the Atlantic hurricane activity was strongly related to West African rainfall (cf. Fink *et al.*, 2010).

Interannual SST variations in the eastern tropical Atlantic Ocean are known to be related with a dipole response in WAM rainfall; warm SSTs tend to enhance (reduce) rainfall over the Guinea Coast (Sahel) and vice versa (e.g. Janicot, 1992; Rowell *et al.*, 1995). Losada *et al.* (2010) ascribe the rainfall reduction over the Sahel during anomalously warm eastern Atlantic SSTs to a decreased meridional surface temperature gradient and weakened surface convergence over the Sahel. SST variability in the equatorial eastern Atlantic has been linked to the zonal Atlantic Niño mode (e.g. Rodríguez-Fonseca *et al.*, 2009). In a recent paper, Losada *et al.* (2012) suggest an explanation for the non-stationary relationship between SSTs in the eastern tropical Atlantic and the dipole response in the WAM region that diminished after the 1970s; they suggest that the emerging anticorrelation between Atlantic and Pacific Niño events since the late 1970s (Rodríguez-Fonseca *et al.*, 2009) caused a monopol-type response over the WAM region. Since the late 1970s, Pacific Niño events determined the Sahelian rainfall anomaly, overriding the Sahel rainfall enhancement signal of the concurrent Atlantic Niña event. In the same year, rainfall over the Guinea Coast was also reduced due to the adjacent cold Atlantic waters. This is consistent with Janicot *et al.* (2001) who noted that the anticorrelation between rainfall in the Sahel and Pacific El Niño Southern Oscillation (ENSO) indices in the northern summer varied in their investigation period 1945–1993. Physically, the impact of Pacific SST anomalies on Sahel rainfall has been assigned to a Gill–Matsuno-type response to SST-induced anomalous tropospheric diabatic heating that impact upper tropospheric outflow and vertical motion over the Sahel region (e.g. Losada *et al.*, 2012).

Other work suggests impacts of SST variations in the Indian Ocean (Bader and Latif, 2003; Giannini *et al.*, 2003; Hagos and Cook, 2008) or in the Eastern Mediterranean Sea (EMS) (Rowell, 2003; Fontaine *et al.*, 2009). The warming trend in the Indian Ocean has been related to the strong Sahel drought in the 1970s and 1980s. Rowell (2003) suggests that warmer SSTs in the EMS enhance moisture fluxes across the Sahara that increase surface moisture convergence in the WAM precipitation zone. Subsidence, mean sea level pressure, and the strength of the Etesian winds in the eastern Mediterranean have been shown to be related to Indian Monsoon rainfall activity (Rodwell and Hoskins, 1996; Raicich *et al.*, 2003), thus representing a potential physical link explaining the weak statistical relation between the Indian and West African monsoon rainfall (Ward, 1998). Despite the wealth of studies on teleconnections between WAM and remote ocean-only or ocean–atmosphere state indices, the results are disperse in terms of the relative roles of teleconnection mechanisms and seem to vary depending on the investigation period, but also on the area and source of precipitation data used to define rainfall.

The aim of this work is to statistically reassess the relative roles of known remote climate variability patterns for WAM rainfall, divided into three regions of West Africa [namely West Sahel (WS), Central Sahel (CS), and Guinea Coast (GC)], for the extended period 1921–2009. Novel aspects are the consideration of many indices of climate variability, including the hitherto rarely used index of the AMM in the context of WAM studies, as well as the use of a particularly homogeneous station rainfall data set covering an almost 90-year period. Furthermore, the study focuses on the evolution of statistical relationship over both various time window lengths for fixed starting years and starting years for fixed time window length, indicating potential non-stationary behaviour of these relationships. As in earlier studies (Janicot *et al.*, 1996; Ward, 1998; Rowell, 2003), a distinction is made between interannual and decadal time scales. The relative roles of the explanatory climate state variables for the explanation of WAM variability are assessed by means of a multi-linear correlation analysis.

The dataset and analysis methods are described in Section 2. Section 3 focuses on the results of the linear correlation between WAM and the selected indices of climate variability. Section 4 presents the correlations patterns obtained with the multi-linear correlation analysis. Finally, the results are summarized and discussed in Section 5.

2. Data and methods

2.1. West African rainfall indices

In this study, the station rainfall database described in Fink *et al.* (2010) is utilized. It consists of monthly rainfall data from 37 stations across tropical West Africa starting in 1921 (Figure 1(a)). Fink *et al.* (2010) used the rainfall data from stations located within three regions to derive a standardized precipitation anomaly index for these areas. Their climatological reference period (mean state) was 1950–1990. The selected regions are the WS, CS, and GC, as shown in Figure 1(a). Stations within these regions have been found to exhibit homogeneous interannual to decadal rainfall variations (Nicholson and Palao, 1993). Compared to Fink *et al.* (2010), the database used in this study has been extended to 2009 and a few missing data have been recovered in earlier years. As outlined in Fink *et al.* (2010), one advantage of the data set used in their study is the rather consistent data availability over time. Furthermore, the subset of 7, 14, and 16 stations used for the WS, CS, and GC nicely reflects June–September (JJAS) rainfall anomalies in these regions when compared to the Climatic Research Unit (CRU) TS 2.1 and the Precipitation Reconstruction over Land (PREC/L) datasets (Fink *et al.*, 2010 and references therein).

Figure 2 illustrates the time series of standardized JJAS rainfall anomalies derived from the station sample within the three regions. The temporal pattern of the WS

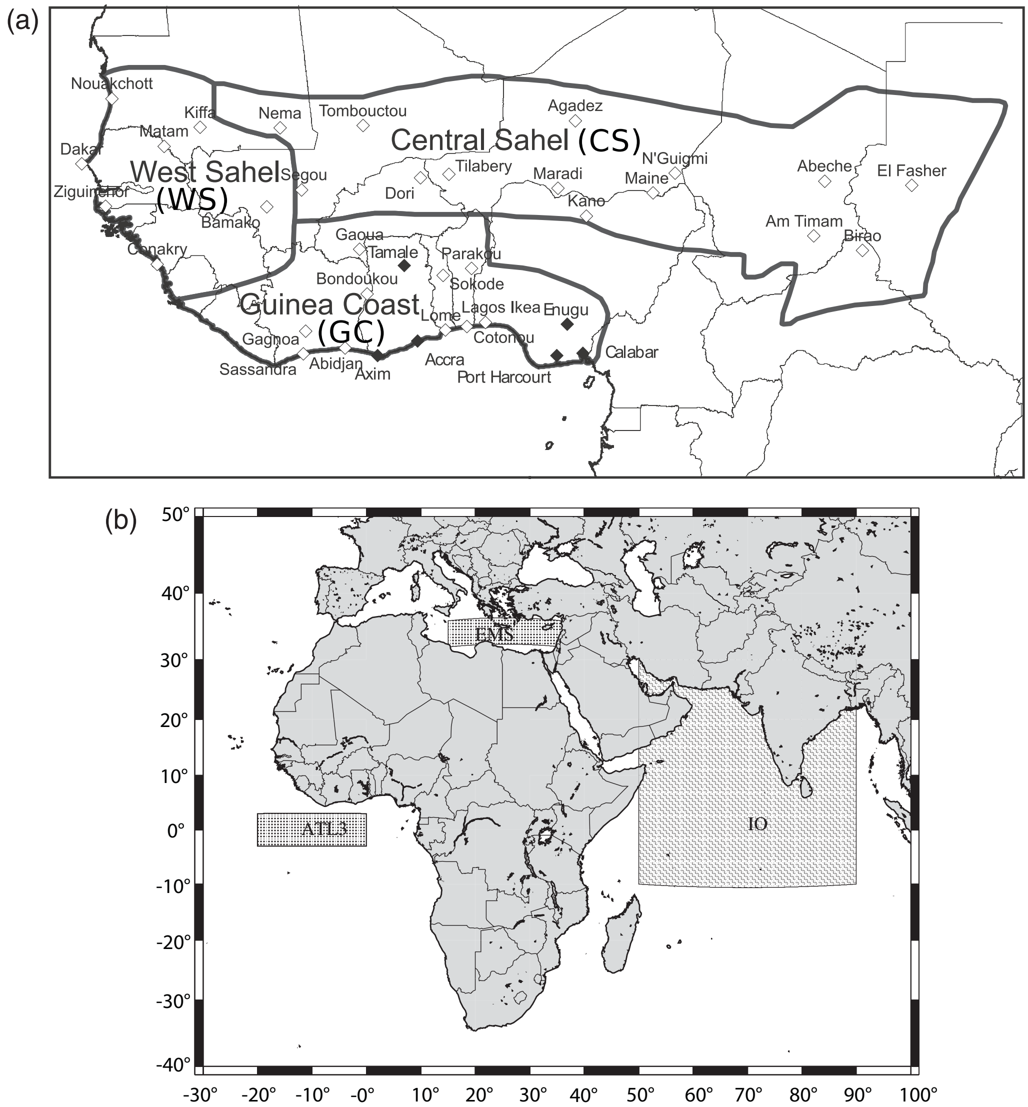

Figure 1. (a) Utilized rainfall stations and definition of subregions after Fink *et al.* (2010); (b) delineation of oceanic areas for which time series of sea surface temperatures have been used; the Indian Ocean (IO), Atlantic zone3 (ATL3), and Eastern Mediterranean Sea (EMS).

rainfall variation (Figure 2(a)) is characterized by a decadal variability with a wet period in the 1930s and in the 1960s, followed by the well-known long-running drought in the 1970s and 1980s (Nicholson and Palao, 1993; Rowell *et al.*, 1995; Ward, 1998; Janicot *et al.*, 2001). On decadal time scales, the CS (Figure 2(b)) exhibits similar rainfall variations when compared to WS. The JJAS rainfall variability in GC region is quite different from the previous two regions; the variability of JJAS rainfall occurs mostly on the interannual time scale (Figure 2(c)), whereas the two Sahelian regions are dominated by decadal rainfall variations. The station rainfall data can be downloaded from http://www.geomet.uni-koeln.de/en/general/the-institute/daten/.

2.2. Indices and time series used in the correlation analyses

In this study, various climate state indices were employed in uni- and multivariate linear regression analyses. Unlike otherwise stated, the indices were available for the entire investigation period, 1921–2009. The SST anomaly in the Niño 3.4 region (5°S–5°N; 120°–170°W, hereafter N3.4) is used to characterize the state of ENSO. In an ENSO warm event (i.e. El Niño), the index is positive, whereas it is negative during ENSO cold events (i.e. La Niña). The N3.4 index used here was computed from SST values from the Hadley Centre Sea Ice and Sea Surface Temperature (HadISST) data set, averaged over the N3.4 region; these SST values are available at http://www.esrl.noaa.gov/psd/gcos_wgsp/Timeseries/Data/nino34.long.data. The N3.4 index is then computed by calculating anomalies with respect to the 1950–1979 mean, smoothing the anomalies with a 5-month running mean, and normalizing the smoothed anomalies by their standard deviation over the climatological period 1950–1990. More details about this ENSO index can be found in Trenberth and Stepaniak (2001). Other ENSO measures used in this study are the Southern Oscillation

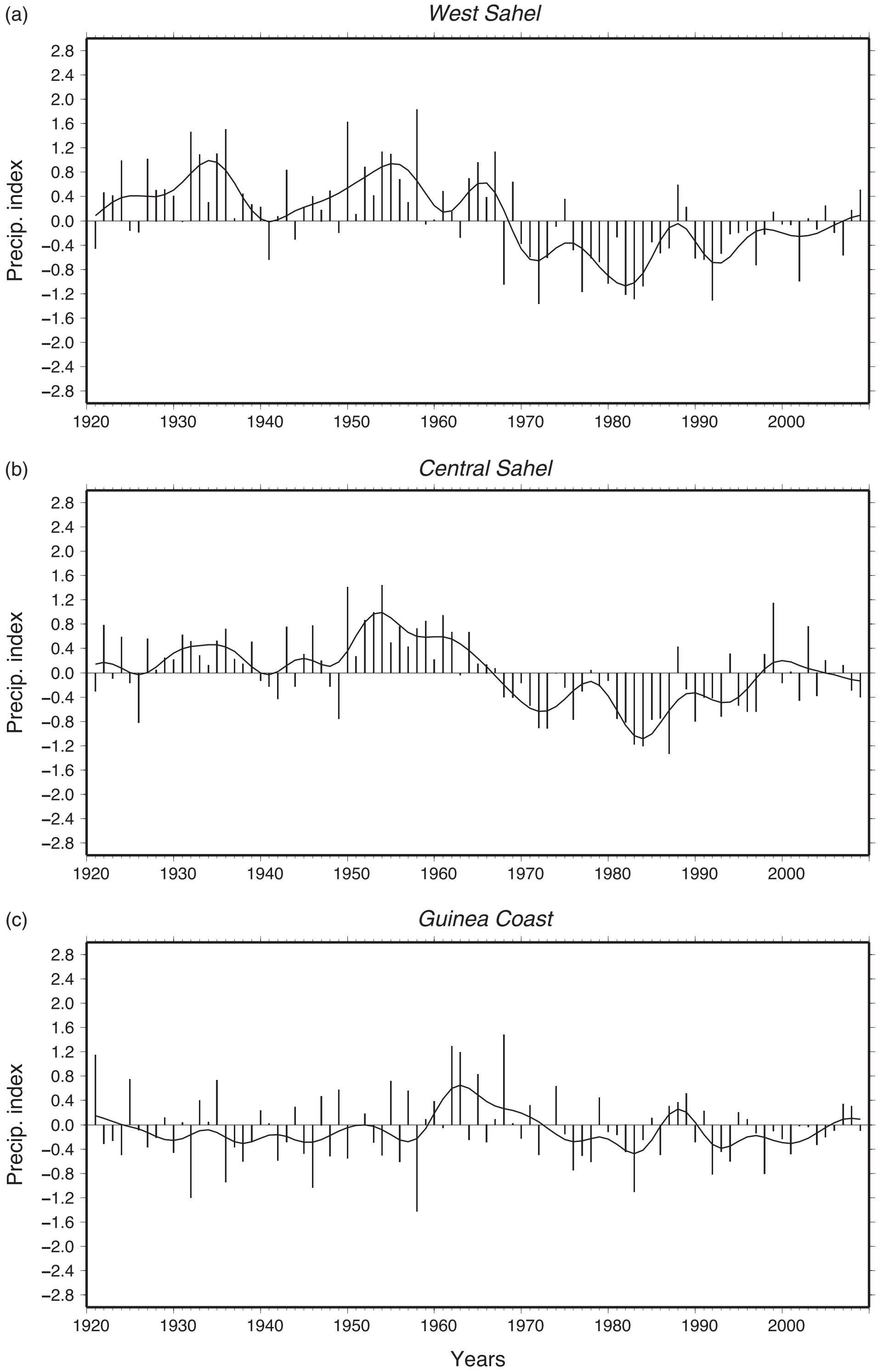

Figure 2. Time series from 1921 to 2009 of the June–September standardized precipitation indices for (a) West Sahel, (b) Central Sahel, and (c) Guinea Coast. The smooth curves were calculated using a Butterworth low-pass filter with a half power period of 8 years. The three regions are mapped in Figure 1(a). [Correction added on 19 February 2014 after original online publication: in Figure 2 the values on the y-axis have been corrected.]

index (SOI), obtained from the National Center for Atmospheric Research (NCAR) Climate and Global Dynamics (CGD) Climate Analysis Sections (CAS) at http://www.cgd.ucar.edu/cas/catalog/climind/SOI.signal.ascii, and the Oceanic Niño Index (ONI) available since 1950 from http://www.cpc.ncep.noaa.gov/products/analysis_monitoring/ensostuff/ensoyears.shtml.

The SOI was computed using the difference of normalized monthly mean sea level pressure anomalies at Tahiti and Darwin with normalization factors based upon annual means for the 1951–1980 period to maximize the signal-to-noise ratio as described in Trenberth (1984). The ONI is very similar to the N3.4 index. Differences are the smoothing (3-month running mean), the reference period (1970–2000), the omission of standardization, and the source of SST data [Extended Reconstructed Sea Surface Temperature (ERSST.v3b)].

The AMO is a basin-scale mode of observed multi-decadal climate variability with alternative warm and cool phases over large parts of the North Atlantic Ocean where the AMO signal is most pronounced (Enfield *et al.*, 2001). The AMO index was obtained from http://www.esrl.noaa.gov/psd/data/timeseries/AMO/ and is based on the Kaplan SST data set at a resolution of $5^{\circ} \times 5^{\circ}$ latitude–longitude. The Atlantic SSTs are averaged over 0°–70°N and the entire time series of the anomalies from the base period 1951–1980 is de-trended. Positive AMO values are indicative of a warmer North Atlantic Ocean.

The AMM describes the basin-wide covariation of SSTs and near-surface winds. This coupled ocean–atmosphere mode is most pronounced in the tropical Atlantic Ocean where it is associated with an SST dipole straddling the equator. The AMM index is calculated by applying Maximum Covariance Analysis (MCA) to SSTs and the zonal and meridional components of the 10 m wind field over the period 1950–2005 from the National Center for Environmental Prediction/National Center for Atmospheric Research (NCEP/NCAR) reanalysis (Chiang and Vimont, 2004). MCA is a method that isolates the most coherent pairs of spatial patterns and their associated time series by performing an eigen analysis on the temporal covariance matrix between two geophysical fields. The AMM index time series used here was calculated via projecting observed SSTs onto the spatial structure of SSTs resulting from the MCA. AMM data used here cover the period 1948–2009 and are available at http://www.esrl.noaa.gov/psd/data/timeseries/monthly/AMM/ammsst.data. A positive AMM index value indicates warmer SSTs north of the equator and stronger cross-equatorial flow from the Southern into the Northern Hemisphere (NH).

The Pacific Decadal Oscillation (PDO) index is defined as the leading principal component of the monthly SST variability of the Northern Pacific (poleward of 20°N) for the period between 1900 and 1993. The globally averaged monthly mean SST anomalies are removed to separate this pattern of variability from any 'global warming' signal that may be present in the data; more details can be found in Trenberth and Hurrell (1994) and Zhang *et al.* (1997). Updated standardized values for the PDO are available at http://jisao.washington.edu/pdo/PDO.latest. A positive PDO is associated with a warmer tropical central Pacific and colder extratropical northwest Pacific.

The Indian Ocean Dipole (IOD) is a coupled ocean–atmosphere phenomenon in the Indian Ocean. Anomalous cooling of SSTs in the southeastern equatorial Indian Ocean and anomalous SST warming in the western equatorial Indian Ocean characterize a warm or positive IOD phase (Saji *et al.*, 1999). During the warm phase, the climatological equatorial surface westerlies blowing towards the Maritime Continent are weakened or reversed. The IOD index is computed from HadISST data (Rayner *et al.*, 2003). It represents the anomaly of the gradient of SSTs (reference period 1950–1990) between the western (50°–70°E and 10°S–10°N) and eastern (90°–110°E and 10°–0°S) equatorial Indian Ocean.

The HadISST data was also used to calculate area-averaged absolute SST values for the following oceanic regions (Figure 1(b)): the Indian Ocean (hereafter IO: 50°–90°E, 10°S–30°N), the EMS (15°–36°E, 32°–36°N) and the Atlantic 3 region (hereafter ATL3: 0°–20°W, 3°S–3°N).

Finally, the all Indian monthly and seasonal (June–September) rainfall series available from http://www.imd.gov.in/section/nhac/dynamic/data.html was used to calculate an All Indian Rainfall (AIR) index normalized using the climatological period 1950–1990. The AIR is thus comparable to the West African indices, reflecting the JJAS anomalies of monsoon rains over India.

Figure 3 illustrates the time series of the indices of climate variability that are related to WAM rainfall in the following analyses. It is evident from Figure 3 that some indices show more pronounced decadal variability than others (e.g. AMO and AMM, Figure 3(b)). The area-averaged SSTs indices (Figure 3(c)) exhibit a recent warming trend. Finally note the out-of-phase behaviour between N3.4 and SOI (Figure 3(a)).

2.3. Statistical methods

For describing the straight-line relationship between remote indices of climate variability and WAM rainfall shown in the later sections, several statistical methods were used. The linear correlation analysis is first employed to evaluate Pearson's linear correlation coefficient and percentage of variance explained (PVE) between the remote climate indices and WAM rainfall. The 'triangle representation' used in Fink *et al.* (2010) was chosen to illustrate the correlation coefficient over all possible combinations of starting dates and time window lengths.

One aspect of this analysis is the use of both unfiltered and filtered data. The low and high pass Butterworth filters (Butterworth, 1930) with a half power periods of 8 years were applied to both time series before the calculation of the linear correlation. The low-pass filtered time series are thus representing fluctuations of 8 years and longer (i.e. decadal time scale) and the high-pass filtered data are reflecting interannual variability. The critical values of the significance levels for ordinary correlations, calculated by an F-test Taubenheim (1969), are used to check the significance of calculated linear correlation. We have then used both the standard degree of freedom (hereafter SDOF) based on the total number of data pairs that enter the correlation, and the (usually) smaller effective degree of freedom (hereafter EDOF)

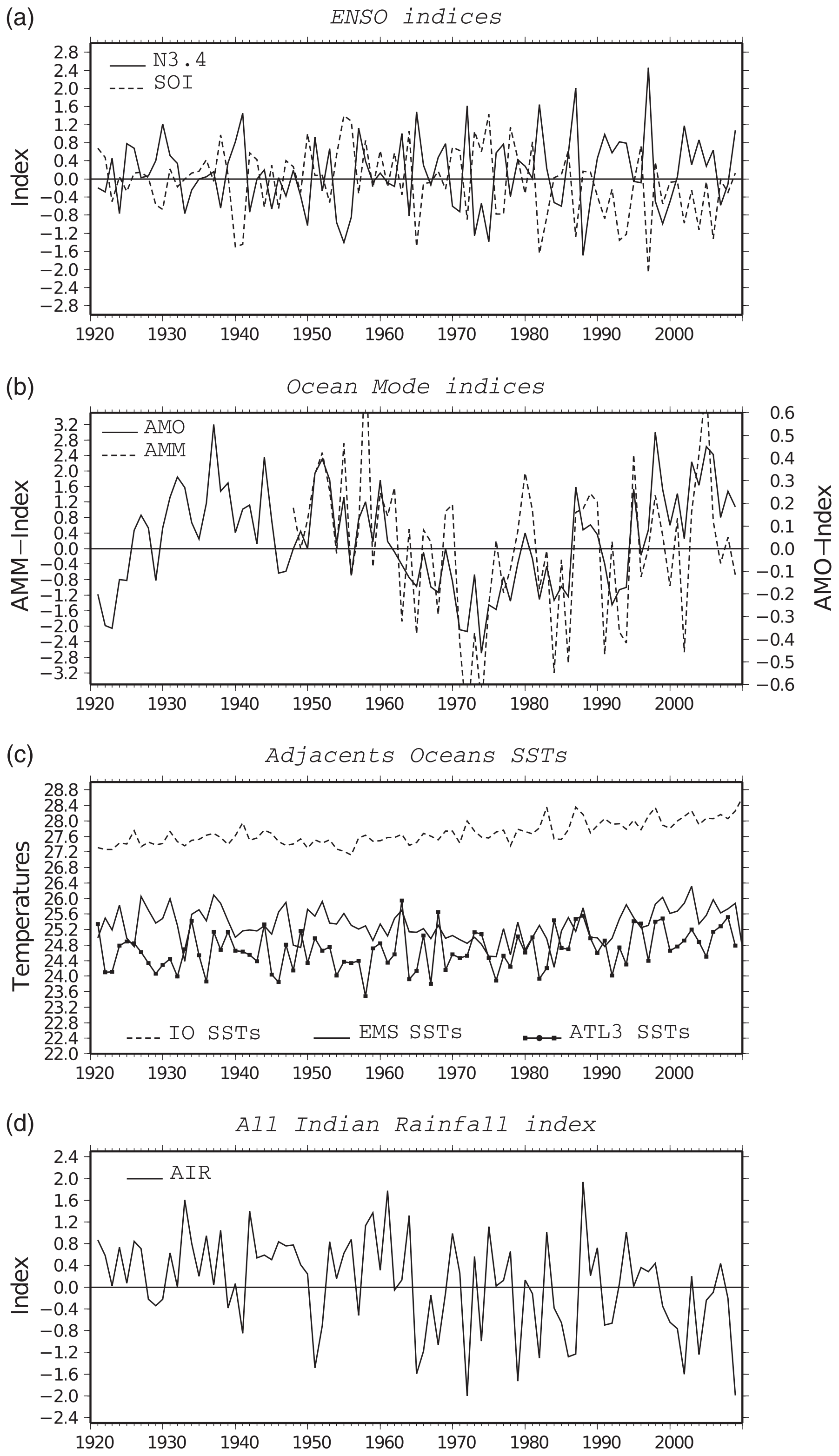

Figure 3. Time series of the June–September indices of climate variability for the period 1921–2009: (a) N3.4 and SOI (standardized, no units), (b) AMO and AMM (period 1948–2009) both in °C, (c) IO SSTs, EMS SSTs and ATL3 SSTs in °C, and (d) the All Indian Rainfall Index (standardized, no units).

as described in Fink and Speth (1997), which takes autocorrelations into account.

In Section 4, multiple linear correlation analysis is computed. The stepwise regression approach Efroymson (1960) has been used to identify the best choice of predictive variables. This approach is applied by starting with no variables in the model, and then by building up the model in a stepwise fashion. The explanatory variable

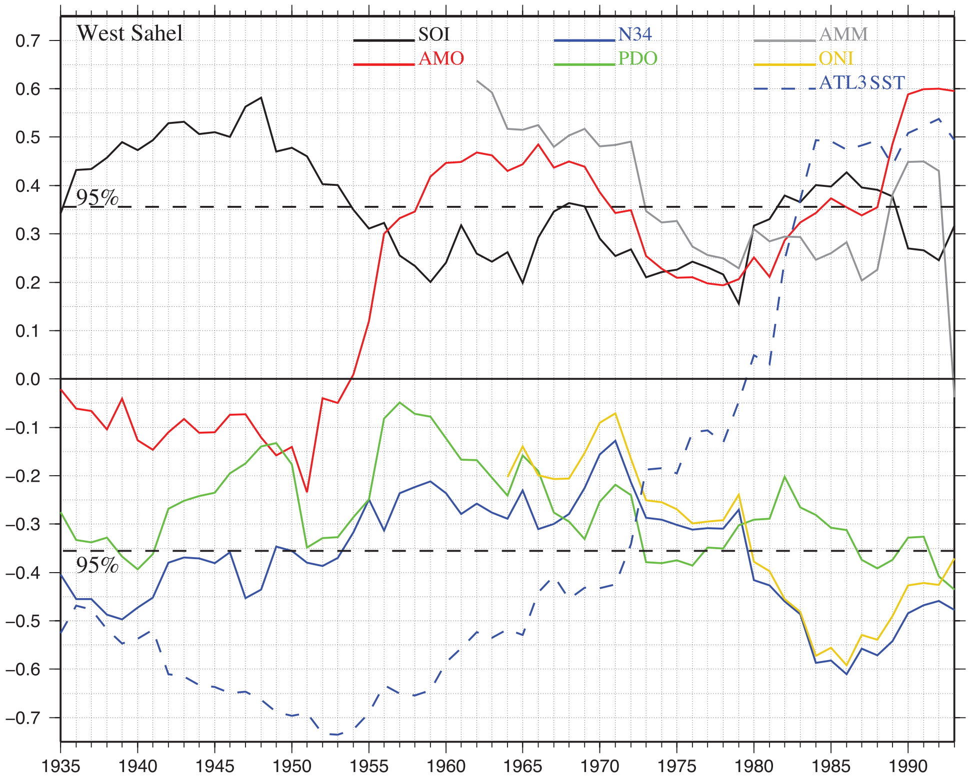

Figure 4. Time evolution of the correlations between seven indices of climate variability and the June–September West Sahel precipitation index using a 31-year moving window. The correlation value for 1935, for instance, relates to the period 1921–1951. The horizontal dashed lines represent the 95% significance level according to the F-test using the SDOF.

that exhibits the highest correlation to the dependent variable in the model is first included, then the next most highly correlated is added, allowing for the first two explanatory variables in the model, and keep adding explanatory variables until no further variables explain significant amounts of variance. In this approach, it is possible to delete a variable that has been included at an earlier step, but is no longer significant, given the explanatory variables that were added later. The approach used here is achieved by using the Akaike Information Criterion (AIC) techniques (Akaike, 1974), which is a measure of the relative goodness of fit of a statistical model. For testing the significance of the connection of multi-linear correlations, the critical values of the significance level given by the Fisher normal distribution are used. Finally for a better interpretation of results obtained from multi-linear correlation, the relative importance for each predictor is assessed by using the metric method proposed by Feldman (2005) called the proportional marginal variance decomposition (PMVD). For more information about the suitability of the PMVD method compared to the others the reader is referred to Grömping (2006).

3. WAM rainfall and indices of climate variability

One focus of this study is the investigation of the behaviour of the teleconnections over time. Figure 4 shows the time evolution of the correlation coefficients between mean JJAS WS rainfall index and seven remote climate indices computed for a 31-year running window that was moved over the investigation period between 1921 and 2009. It is evident from Figure 4 that the correlations are non-stationary to different degrees. One outstanding example is the ATL3 index. It changed from significant negative correlations of larger than −0.7 in the early 1950s to significantly positive correlations of about 0.5 in the last decade of the investigation period. Using the significance test proposed by van Oldenborgh and Burgers (2005) based on creating randomly 1000 time series with the same 89-year correlation and using a window length of 31 years, the changes in the running correlation between the ATL3 index and WS rainfall are significant. It reflects the change from a concurrent occurrence of a warm tropical east Atlantic and a dry Sahel in the early part of the investigation period to a simultaneous occurrence of a warm tropical east Atlantic Ocean and a wet Sahel in recent decades as referred to in Section 1. A second significant non-stationary correlation is that between the AMO index and WS rainfall. For 31-year windows centred on years between 1950 and 1960, the linear correlation coefficient rose to statistically significant values between 0.4 and 0.5. After a drop to insignificant values during the Sahelian drought in the 1970s, the correlation recovered in recent decades to the highest values calculated (0.6). For the given window length of 31 years, the AMO index cannot represent the

Table 1. Correlation coefficients between remote indices of climate variability and WS, CS, and GC rainfall indices.

	WS	CS	GC
AMO	**0.281**	**0.287***	−0.069
AMM (1948–2009)	**0.470***	**0.372***	−0.116
IOD	**−0.300***	**−0.230**	0.056
SOI	**0.349***	**0.283**	0.016
PDO	**−0.300***	**−0.378***	−0.154
N3.4	**−0.352***	**−0.339***	−0.001
ONI (1950–2009)	**−0.32**	**−0.353***	−0.020
IO SST	**−0.483***	**−0.428***	−0.100
EMS SST	**0.263**	**0.447***	−0.027
ATL3 SST	**−0.348***	**−0.250**	**0.524***
AIR	**0.316***	**0.329***	−0.166

Correlation coefficients in bold (with an asterisk) are significant at the 95% (99%) significant level according to the F-test using the SDOF.

AMO that fluctuates on time scales of about 60 years (Kerr, 2000; Enfield *et al.*, 2001). Thus, this significant non-stationary correlation reflects the changes in the covariability between interannual SST anomalies in the North Atlantic (cf. Figure 3(b)) and WS rainfall.

The absolute value of the correlation coefficient of WS rainfall and the three ENSO indices N3.4, ONI, and SOI also varies over the study period between statistically insignificant values of 0.2 and significant values in excess of 0.5. The former two indices reach a value of −0.6 for 31-year windows centred on the years around 1985. However, none of the remaining time evolutions of the correlation coefficients in Figure 4 passed the significance test of non-stationarity. Finally, Table 1 presents a summary of correlation coefficients between all remote indices of climate variability and WAM precipitation index for the entire period of investigation (1921–2009, except for the AMM and ONI, which are only available for the indicated period). All climate indices show correlations with Sahel rainfall that exceed the 95% confidence level. For GC, only the ATL3 SSTs yield a significant correlation. Therefore, the results for GC region will only be shown when appropriate.

3.1. Coupled ocean–atmosphere modes, oceanic modes, and WAM rainfall variability

Firstly, the AMO and AMM indexes that are related to the interannual to decadal variability in the Atlantic Ocean are investigated. Figure 5 shows the linear correlation coefficients between AMO and rainfall for the two Sahelian regions for the period 1921–2009 using a combination of starting dates and time window lengths. The triangle representation of correlations can be interpreted as follows; firstly, moving from the starting dates on the left ordinate horizontally to the right represents correlations at the starting year with increasing time window length. Secondly, moving from the top vertically downward yields correlations for the moving time window denoted on the lower abscissa. The 95% significance based on SDOF (EDOF) is indicated by contours (stippling). All triangle plots were also calculated with linearly de-trended time series; results were quite similar and will not be discussed further.

In the case of WS (Figure 5(a)), a significant positive correlation for time series longer than 40 years is seen for starting years between 1921 and 1940. However, the correlation values between 0.3 and 0.35 are relatively low. After a deterioration of the correlation in the 1960s, a stronger and statistically significant relationship re-emerged after 1975; in this period the correlations exceed 0.5. The latter behaviour is largely due to the interannual variability of SSTs in the Atlantic Ocean north of the equator, but not due to the AMO that apparently causes positive correlations in time series of several decades long (Figure 5(c) and (d)). The CS (Figure 5(b)) exhibits almost identical patterns though the recovery in the correlation is not as pronounced as for the WS.

Similar analyses are shown in the remaining panels of Figure 5, but the time series were subject to low-pass (Figure 5(c) and (d)) and high-pass filtering (Figure 5(e) and (f)) with a half power period of 8 years. For the low-pass filtered ‘triangle correlation plots’, window lengths equal or larger than 40 years have been used in Figure 5 and in all future figures, though correlation coefficients must notwithstanding be interpreted with caution due to the very few cycles of decadal variations that can occur in 40–89-year long time series. Not surprisingly, Figure 5(c)–(f) clearly reveals that the correlation pattern in the unfiltered triangle plots for both regions stems from periods longer than 8 years. With a periodicity of approximately 60 years, the AMO also contributes substantial amount of variance in the shorter multi-decadal periodicity band (not shown). Interannual fluctuations in the AMO index cause significant negative correlations with CS rainfall in the early part of the investigations period (Figure 5(f)), the causes of which are unclear.

Figure 6 illustrates the triangle representation of correlations between the AMM and the WAM over all sampled time windows from 1948 to 2009, corresponding to the available period of the AMM index (cf. Section 2.2). For the WS, both high- and low-frequency variations in the time series of the AMM contribute to the positive and significant correlation in the unfiltered signal (Figure 6(a), (c), and (e)), especially in the first decades after the beginning of AMM data availability in 1948. In contrast to WS, the influence of AMM on CS rainfall is only significant on decadal time scales (Figure 6(b), (d), and (f)). This is likely due to the covariability of AMM and AMO on decadal time scales (Figure 3). In summary, AMO and AMM show a positive linear correlation to Sahel rainfall that explained at most 10–25% of its variance. Not surprisingly, the correlation stems from the periods longer than 8 years for AMO, but AMM does show a correlation on interannual time scales for WS, possibly suggesting a closer physical relation between AMM and rainfall in the WS. Interestingly, this correlation seemed to be absent between 1970 and 1990.

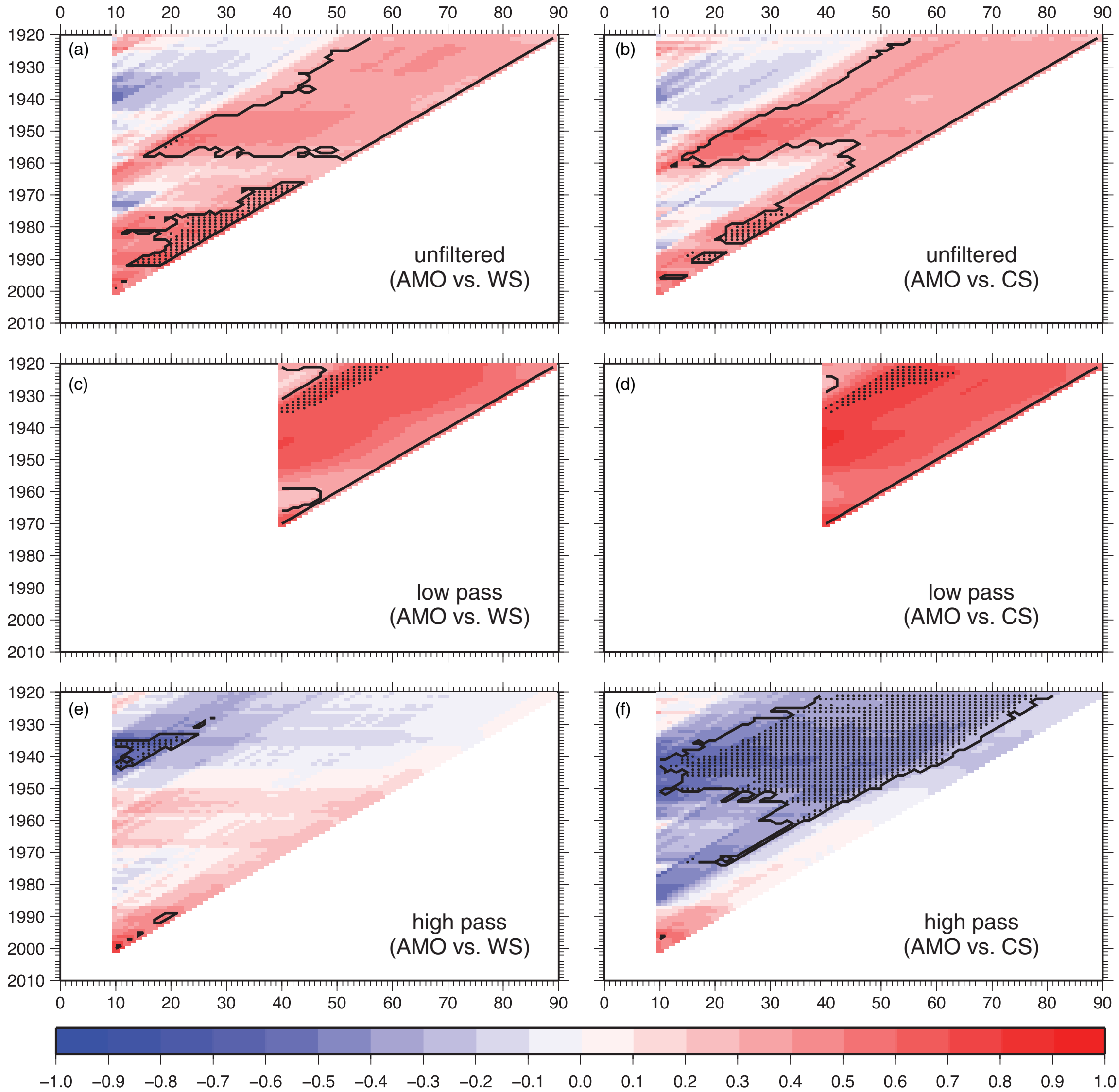

Figure 5. Correlation coefficients between the July–September indices of the AMO and of the standardized rainfall anomalies for West Sahel (left panels) and Central Sahel (right panels), for all starting years (ordinate) and time sample sizes (abscissa). (a, b) Unfiltered component; (c, d) low-frequency component, i.e. longer than 8 years. Here, only window length of ≥40 years is displayed. (e, f) High-frequency component, i.e. shorter than 8 years. Contours (stippling) denote areas above the 95% significance level according to the *F*-test using standard degree of freedom (effective degree of freedom).

Similar analyses of the linear relationships between WAM rainfall and indices of coupled ocean–atmosphere modes such as PDO and IOD have been performed but are not shown here. The PDO is significantly negatively correlated with Sahel rainfall for long time series. The relation to the CS seems to be somewhat stronger. The IOD on the other hand, gives low and largely not significant correlation with CS rainfall. The only significant but still low correlations are obtained with WS rainfall for earlier years and for long time series and are related to decadal trends.

3.2. Correlation between ENSO activities and the WAM

In order to investigate the variation of WAM rainfall-ENSO correlations, the analyses of the correlation of all possible combinations have been performed between WAM rainfall and several ENSO indices (cf. Section 2). Figure 7(a) and (b) shows the correlation patterns between the N3.4 index and WAM rainfall with the unfiltered data. In WS and CS, the N3.4 index is negatively correlated with rainfall for long sample periods starting between the 1920s and 1950s and more recently also for shorter sample period lengths. The PVE for long-term sample periods (60–89 years) starting in the first half of the 20th century is about 10%, which is low but statistically significant. The statistical significant correlation between N3.4 and Sahel rainfall largely stems from the high-frequency interannual fluctuations (Figure 7(c) and (d)), but the decadal time window also contributes (Figure 7(e) and (f)). As the PDO is known to be modulated by ENSO on interannual time scales (Newman et al.

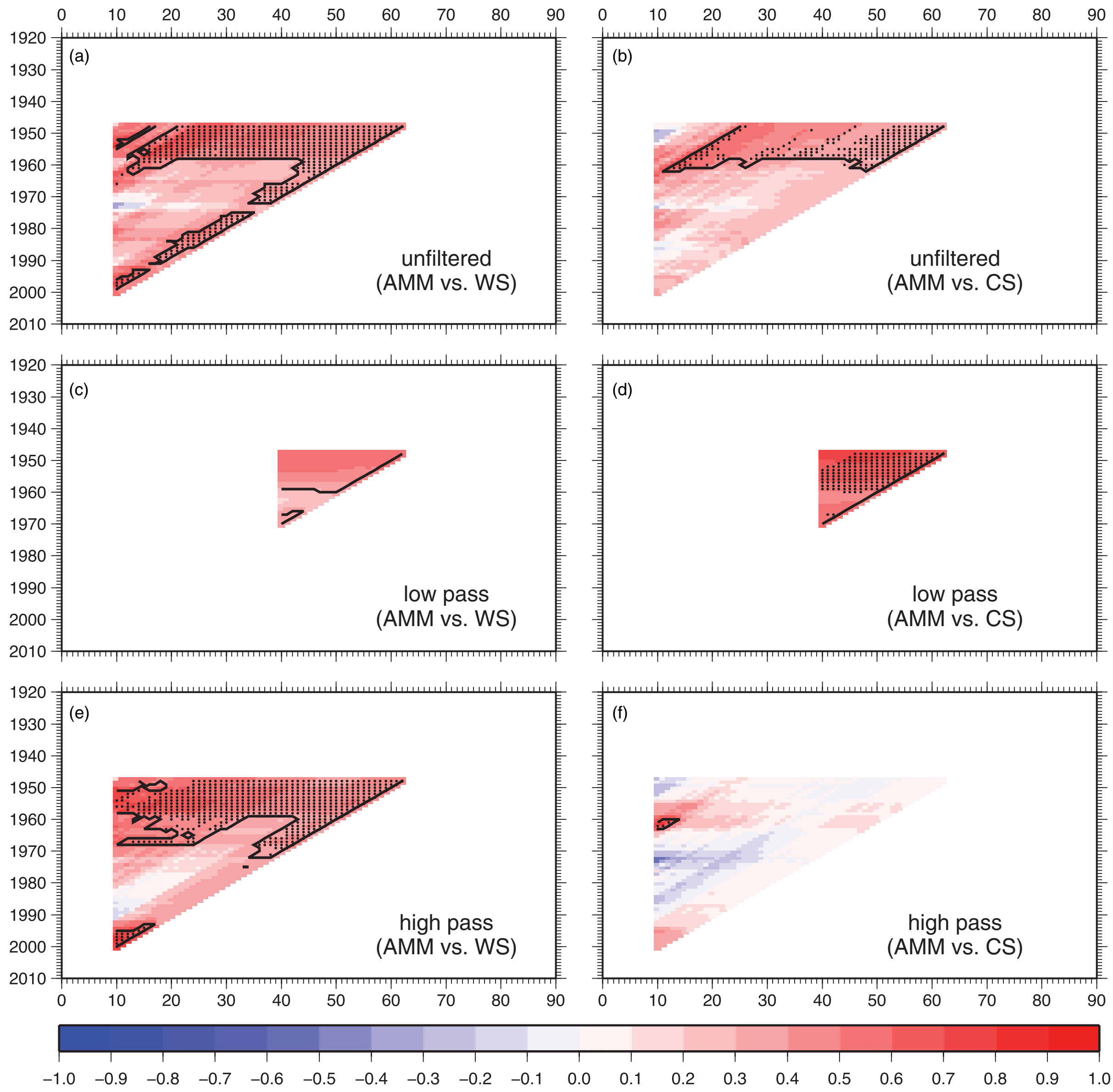

Figure 6. Correlation coefficients between the July–September indices of the AMM index and of the standardized rainfall anomalies for West Sahel (left panels) and Central Sahel (right panels), for all starting years (ordinate) and time sample sizes (abscissa). (a, b) Unfiltered component; (c, d) low-frequency component, i.e. longer than 8 years. Here, only window length of ≥40 years is displayed. (e, f) High-frequency component, i.e. shorter than 8 years. Contours (stippling) denote areas above the 95% significance level according to the *F*-test using standard degree of freedom (effective degree of freedom).

2003), this is consistent with the above-mentioned significant negative correlation between the PDO and Sahel rainfall. It appears that the correlation between the N3.4 index and both, WS and CS rainfall, was stronger in the second part of the 20th century (Figure 7(a) and (b)). The N3.4 does not influence the JJAS rainfall variability in the GC; the correlation coefficients in all periods are low and not significant (not shown).

Correlation analyses between other ENSO indices and the WAM were performed. The analyses of the ONI influences on WAM rainfall variability show very similar patterns as N3.4, which is not surprising given that the ONI is an oceanic ENSO index obtained from the N3.4 region (not shown). As expected from the opposite sign of the SOI for ENSO warm and cold phases when compared to the N3.4 (cf. Figure 3(a)), the correlation patterns are opposite (Figure 8). However, two differences are worthy to note: (1) the SOI is not as highly related to rainfall variations in CS (Figure 8(b)) and (2) a decline in the correlation is observed in recent decades, especially on the interannual time scales (Figure 8). Janicot *et al.* (1996) pointed to a significant correlation between SOI and Sahel rainfall for 1968–1993 that stemmed from the interannual period band. As can be seen in Figure 8(a), this was an unusual period as, prior to 1968 and after 1993, the correlation was not significant, suggesting a potential non-stationary behaviour of the SOI versus Sahel rainfall relationship (cf. Figure 4). In summary,

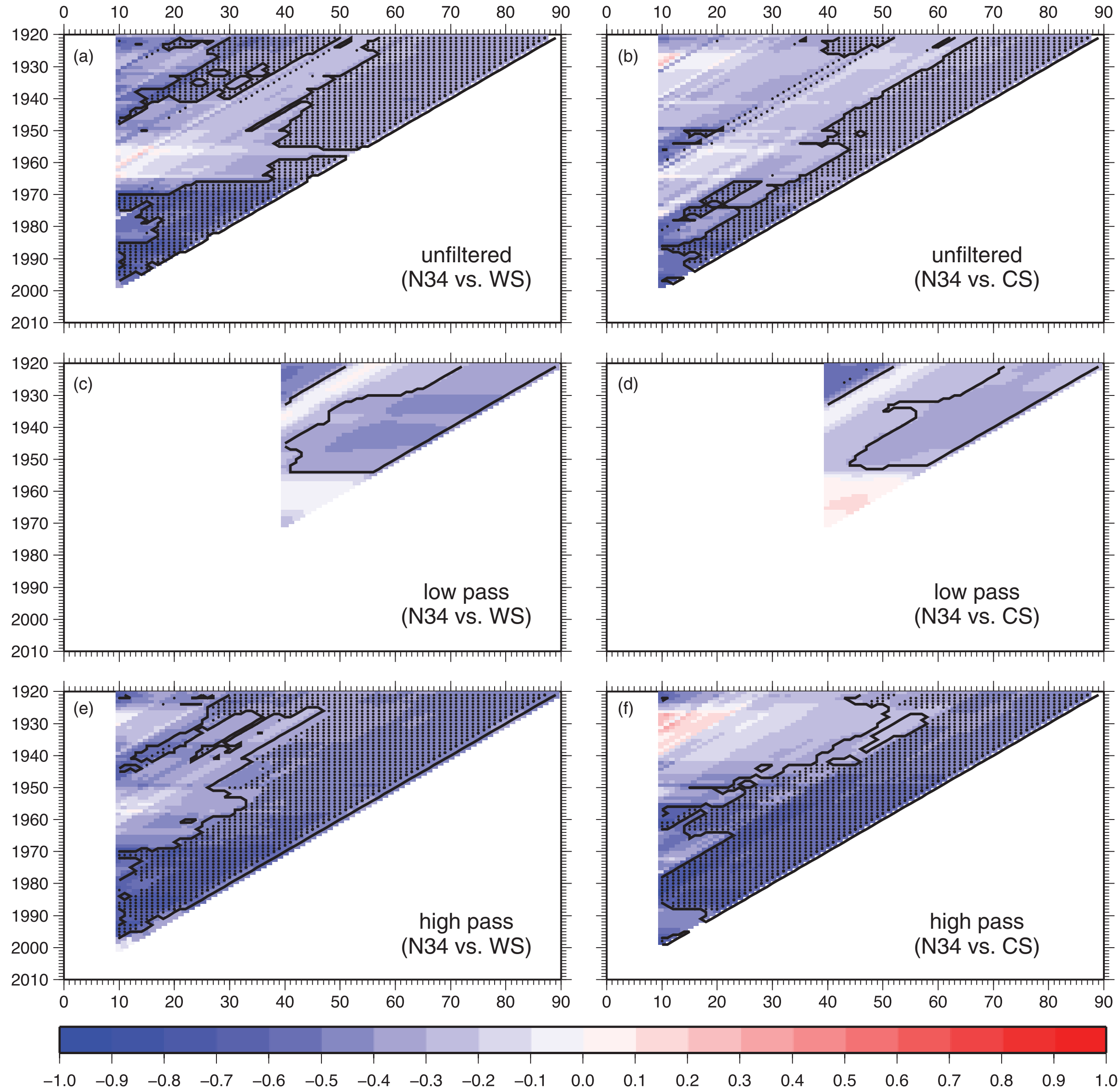

Figure 7. Correlation coefficients between the July–September indices of the Niño 3.4 index and of the standardized rainfall anomalies for West Sahel (left panels) and Central Sahel (right panels), for all starting years (ordinate) and time sample sizes (abscissa). (a, b) Unfiltered component; (c, d) low-frequency component, i.e. longer than 8 years. Here, only window length of $\geq$40 years is displayed. (e, f) High-frequency component, i.e. shorter than 8 years. Contours (stippling) denote areas above the 95% significance level according to the F-test using standard degree of freedom (effective degree of freedom).

the analyses of correlations between the ENSO indices N3.4 and ONI and the Sahel rainfall suggest a particularly robust connection at the interannual time scale in recent years, as pointed out by Ward (1998) and Palmer *et al.* (1992), which is not seen in the SOI. In earlier years, the relation is weaker (Figure 7(a)–(f)).

3.3. SSTs from adjacent oceans and their relation to WAM rainfall

Connections between SSTs from adjacent oceans described in Section 2.2 and the WAM rainfall variability are now investigated. As previously, Figures 9, 10, and 11 describe all possible combinations of correlations between SSTs from adjacent oceans and appropriate West African subregions' rainfall.

Figure 9 presents the correlation pattern between IO SSTs and WS and CS rainfall indices (GC rainfall is not shown because the correlation pattern is not significant). For earlier years starting from 1921 to nearly 1960, the correlations between IO SSTs and rainfall over WS and over CS are negative and significant using both SDOF and EDOF and are relatively high with correlation coefficient on the order of −0.4 to −0.6 using unfiltered data (Figure 9(a) and (b)). These correlations largely result from decadal fluctuations (Figure 9(c) and (d)). Janicot *et al.* (1996) and Bader and Latif (2003) argue that increasing SSTs in the IO were associated with

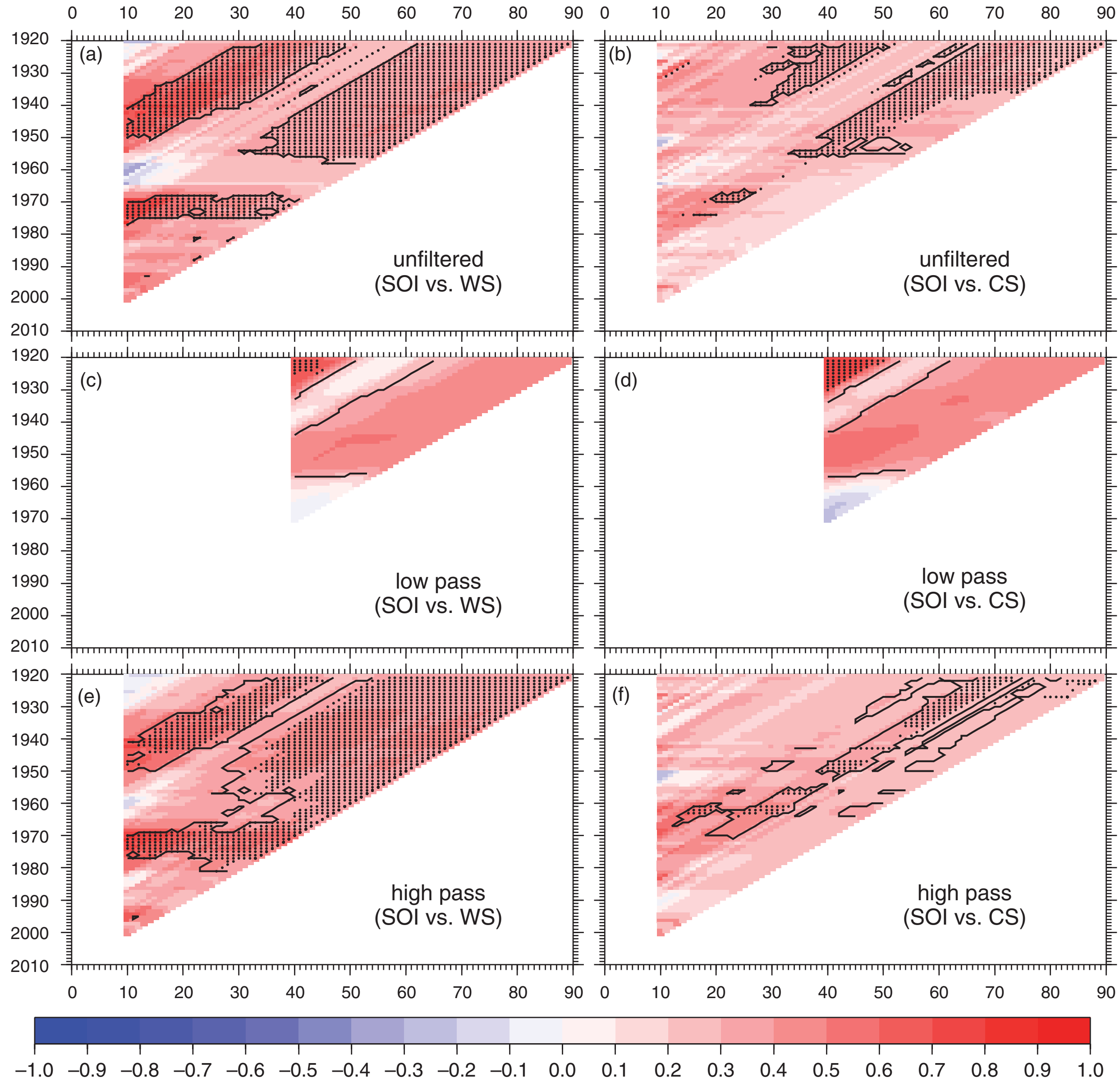

Figure 8. Correlation coefficients between the July–September indices of the SOI and of the standardized rainfall anomalies for West Sahel (left panels) and Central Sahel (right panels), for all starting years (ordinate) and time sample sizes (abscissa). (a, b) Unfiltered component; (c, d) low-frequency component, i.e. longer than 8 years. Here, only window length of ≥40 years is displayed. (e, f) High-frequency component, i.e. shorter than 8 years. Contours (stippling) denote areas above the 95% significance level according to the *F*-test using standard degree of freedom (effective degree of freedom).

a reduction of precipitation in the Sahel. This would explain the observed negative relationship in Figure 9, especially on decadal time scales. In the total signal, significant correlations between Sahel rainfall and IO SSTs are not found for recent years (Figure 9(a) and (b)). This may simply because the significant anti-correlations solely stem from decadal time scales and time series lengths for recent starting years are too short. On the other hand, Figure 9(c) and (b) shows weakening and even inverse correlations for 40–50-year long time series starting in between 1960 and 1970. If this points to a non-stationarity in which the sign of the decadal scale correlation changes is too premature to infer.

Figure 10 describes all possible linear correlations between the EMS SSTs and rainfall over the WS and CS. As can be seen in the unfiltered data in Figure 10(a) and (b), the relation between the EMS SSTs and WS rainfall is overall weak and non-significant, whereas significant correlations are evident for the CS for longer periods starting from the first part of the investigation period. Figure 10(a), (b) (e), and (f) reveals that the relation is strong on interannual time scales in the most recent decades, supporting the findings by Rowell (2003) for the entire Sahel region. Figure 10(c) and (d) suggests an occasionally significant correlation on decadal times scales.

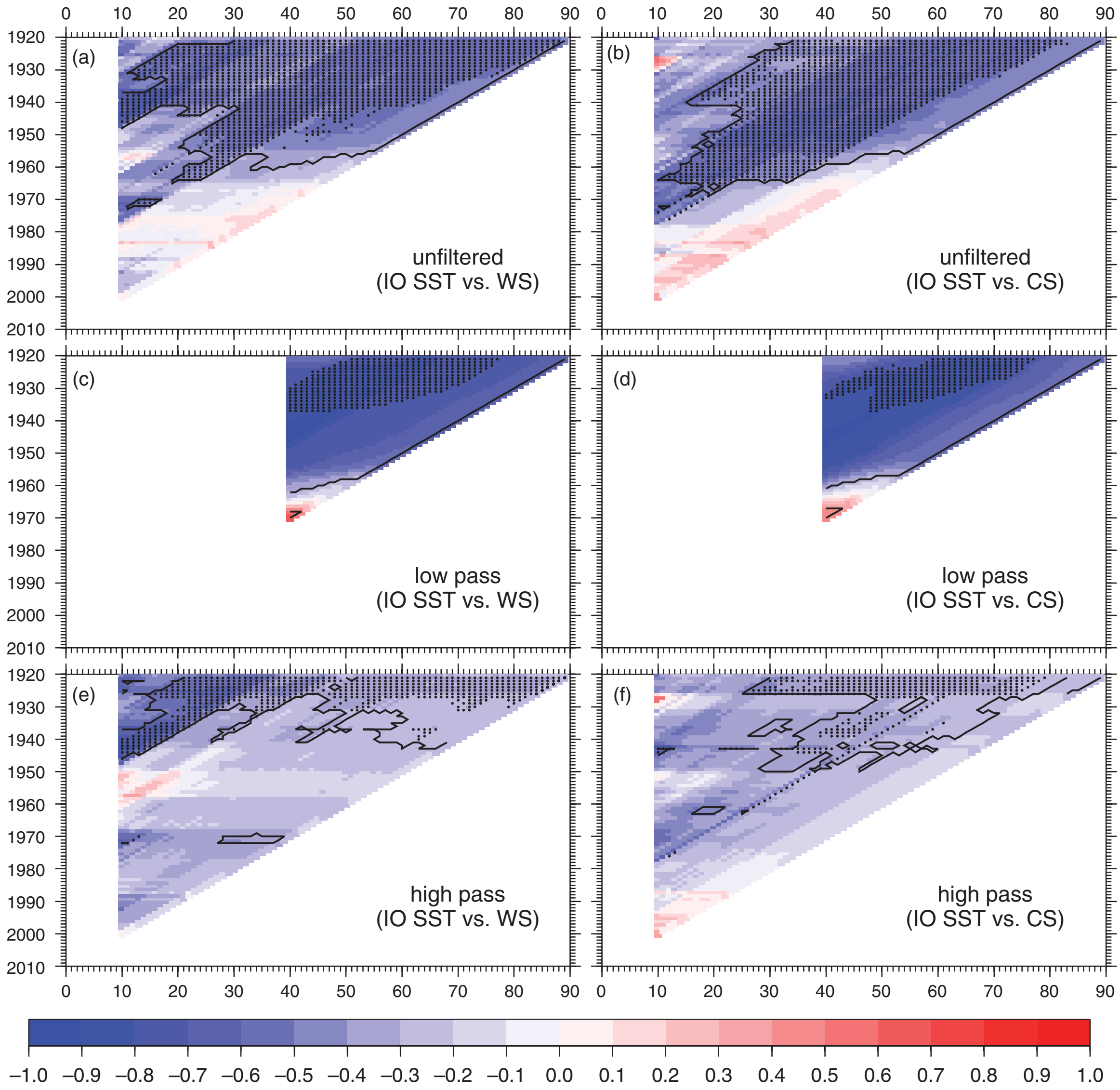

Figure 9. Correlation coefficients between the July–September indices of the Indian Ocean (IO) SSTs and of the standardized rainfall anomalies for West Sahel (left panels) and Central Sahel (right panels), for all starting years (ordinate) and time sample sizes (abscissa). (a, b) Unfiltered component; (c, d) low-frequency component, i.e. longer than 8 years. Here, only window length of ≥40 years is displayed. (e, f) High-frequency component, i.e. shorter than 8 years. Contours (stippling) denote areas above the 95% significance level according to the *F*-test using standard degree of freedom (effective degree of freedom).

The last adjacent ocean forcing is diagnosed by using the ATL3 SSTs. Figure 11 illustrates linear correlations between the ATL3 SSTs and the WS and GC rainfall for all sample times as done previously. No significant relationship between ATL3 SSTs and rainfall in CS is observed. The most salient features in Figure 11 are the strong positive correlations between ATL3 and GC rainfall, and a sign reversal in the correlation to WS rainfall. At the GC, JJAS rainfall is strongly related to ocean temperatures in the ATL3 region at interannual time scales and correlation coefficients exceed 0.6 in the unfiltered analysis (Figure 11(b)). This is consistent with earlier studies (e.g. Fontaine *et al.*, 1998; Paeth and Hense, 2006). Contrary to other findings in the present study, the correlation is robust over the entire investigation period for all time window lengths. For the WS, the correlation changes from negative to positive in the 1970s while being significant before and after this reversal (Figure 11(a)). This sign reversal is evident in the low- and high- frequency band (Figure 11(c) and (d)). A dipole pattern with respect to rainfall anomalies in the Sahel and the GC, has been noted by Nicholson (2008). Such dipole behaviour is consistent with positive (negative) correlations between ATL3 SSTs and rainfall in the GC (WS) regions because it may be related to anomalies in the location of the zonal band of maximum rainfall. Our statistical analyses points to the possibility that the dipole years were more frequent and stronger before about 1970s and weaker and less frequent afterwards. This has been noted in Mohino *et al.* (2011b).

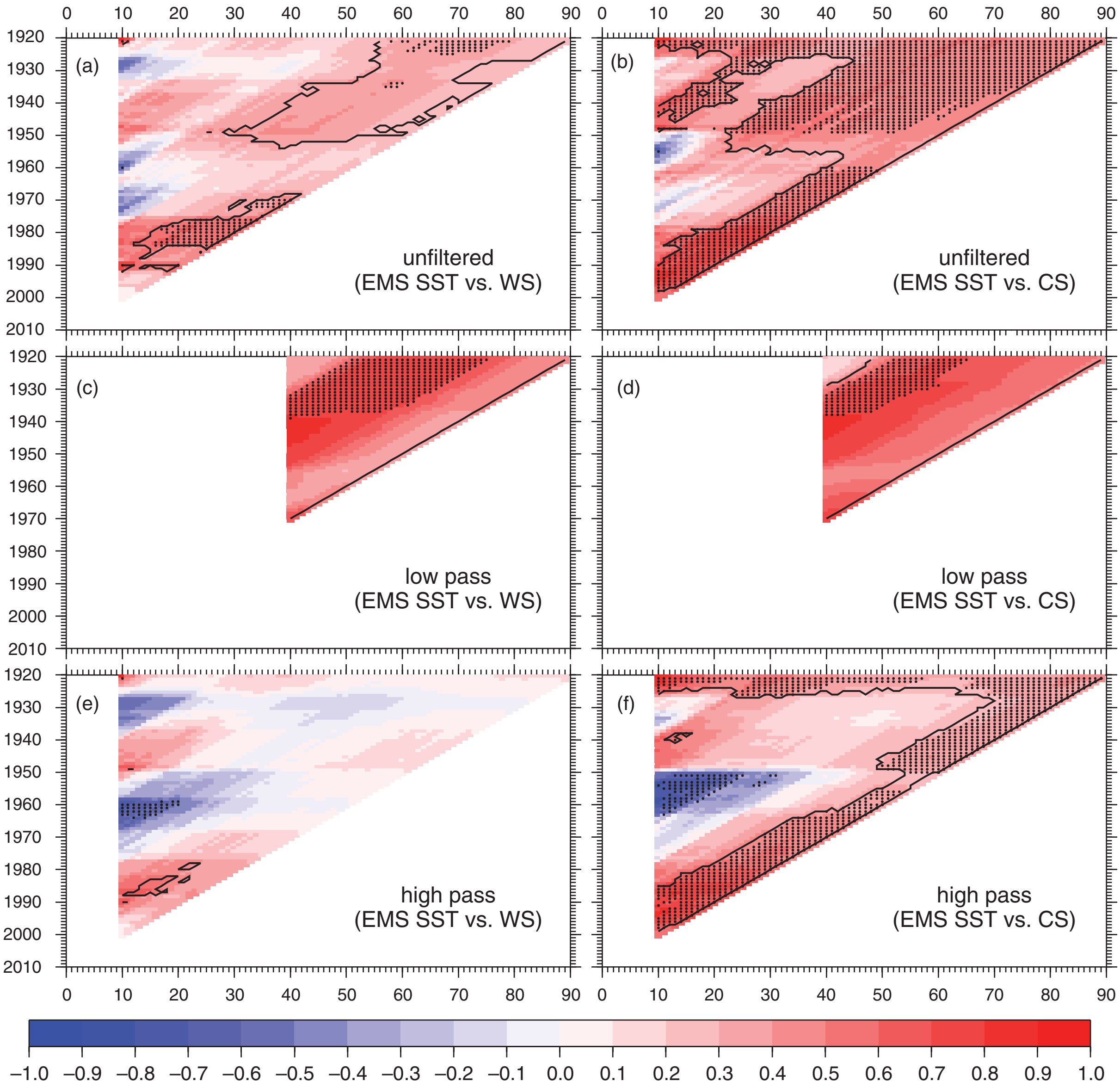

Figure 10. Correlation coefficients between the July–September indices of the Eastern Mediterranean Sea (EMS) SSTs and of the standardized rainfall anomalies for West Sahel (left panels) and Central Sahel (right panels), for all starting years (ordinate) and time sample sizes (abscissa). (a, b) Unfiltered component; (c, d) low-frequency component, i.e. longer than 8 years. Here, only window length of ≥40 years is displayed. (e, f) High-frequency component, i.e. shorter than 8 years. Contours (stippling) denote areas above the 95% significance level according to the F-test using standard degree of freedom (effective degree of freedom).

3.4. Relationship between AIR and the WAM rainfall

The analyses of correlation coefficients between AIR and WS and GC precipitations show different patterns (Figure 12). The relationship with CS is not shown because it is quite similar with the WS pattern. The influence of AIR on WAM variability is mostly established on interannual time scales; the correlations between these two monsoons vary between 0.3 and 0.4, thus explaining only about 10–15% of the variance in WAM rainfall. The high-frequency component shows significant correlations between the AIR index and rainfall in WS for long time series (40–89 years) and for starting years between 1921 and 1960 (Figure 12(e)). However, on the interannual time scale, AIR is positively correlated with WS rainfall and negatively with GC (Figure 12(e) and (f)), though the negative correlation coefficients are smaller and less significant (Figure 12(b) and (f)). For the WS, some significant contributions for the positive correlation are evident on decadal time scales (Figure 12(c)). Ward (1998) provided evidence of a positive correlation between Indian and Sahelian rainfall on the high-frequency time scale. He argued that this positive correlation occurred independent of any association with SSTs, raising the possibility of teleconnection processes internal to the atmosphere or land-atmosphere system. Raicich *et al.* (2003) used precipitation indices for the period 1948–1994 to point out teleconnections between Indian and Sahel rainfall

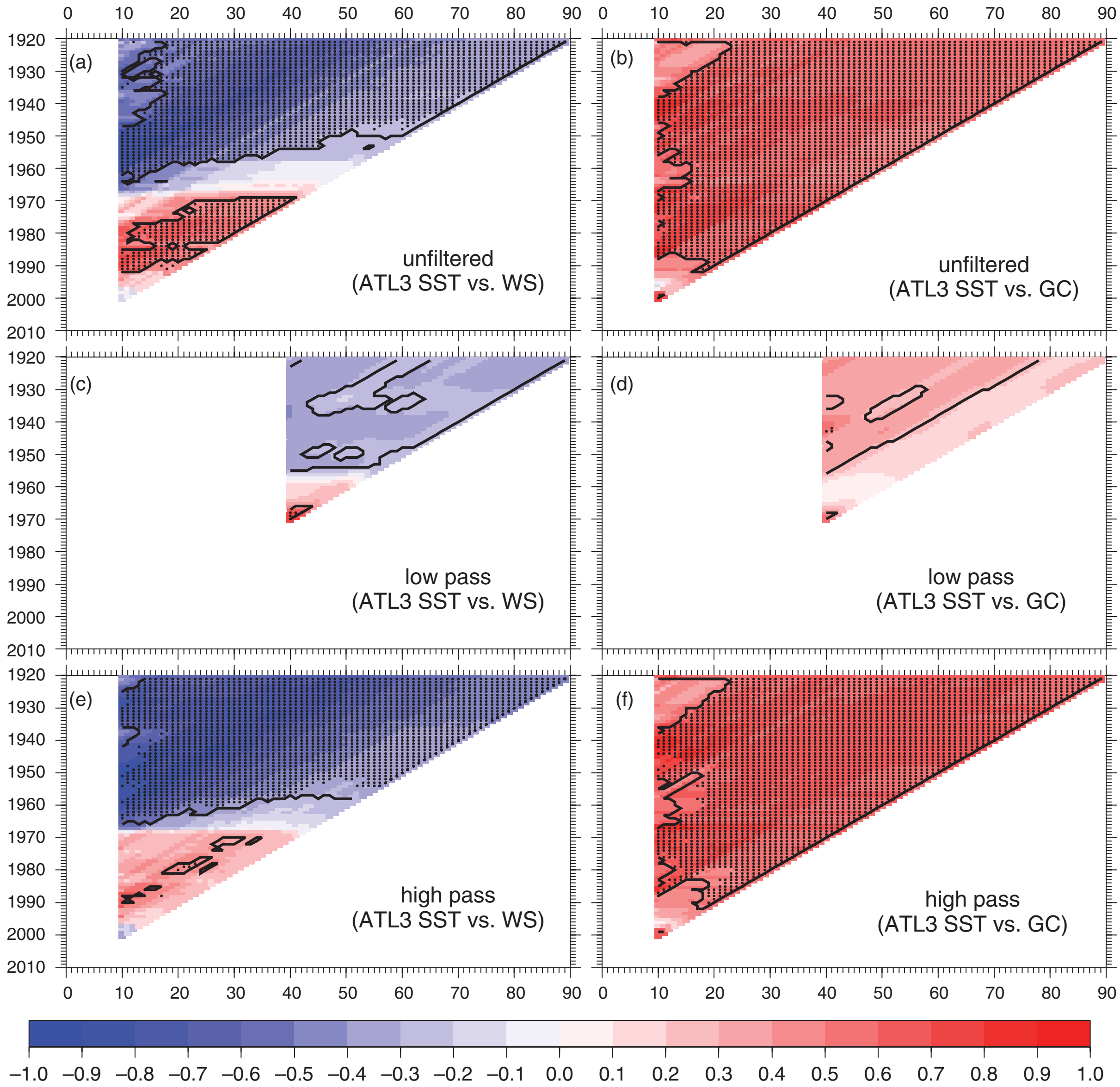

Figure 11. Correlation coefficients between the July–September indices of the Atlantic zone3 (ATL3) SSTs and of the standardized rainfall anomalies for West Sahel (left panels) and Guinea Coast (right panels), for all starting years (ordinate) and time sample sizes (abscissa). (a, b) Unfiltered component; (c, d) low-frequency component, i.e. longer than 8 years. Here, only window length of ≥40 years is displayed. (e, f) High-frequency component, i.e. shorter than 8 years. Contours (stippling) denote areas above the 95% significance level according to the F-test using standard degree of freedom (effective degree of freedom).

on an interannual time scale and based on dynamical processes over the Mediterranean area. Kucharski *et al.* (2009) suggested a simple Gill–Matsuno-type quadrupole response of the atmosphere to a heating anomaly in the equatorial Atlantic region to understand the relationship between African and Indian rainfall. But one interesting observation is the deterioration of this relationship in recent years, with a stronger deterioration observed at the GC (Figure 12(a) and (b)).

4. Multi-linear correlation analysis

The following section outlines the pattern of multi-linear correlations between predictive variables (WAM rainfall) and selected explanatory variables or predictors (indices of climate variability). How a set of explanatory variables is associated with a dependent variable of interest (here the WS, CS, and GC rainfall) is first investigated. Note that AMM could not be included because the regression model was applied to the entire investigation period 1921–2009 and then taken to produce the triangle plots. The aim here is to highlight the time evolution of correlation coefficients depicted from each multi-linear model. The stepwise selection method explained in Section 2.3 is used to choose the best explanatory variables for predicting the WS, CS, and GC rainfall. Table 2 shows the best simultaneous predictors along with their corresponding coefficient of regression for each

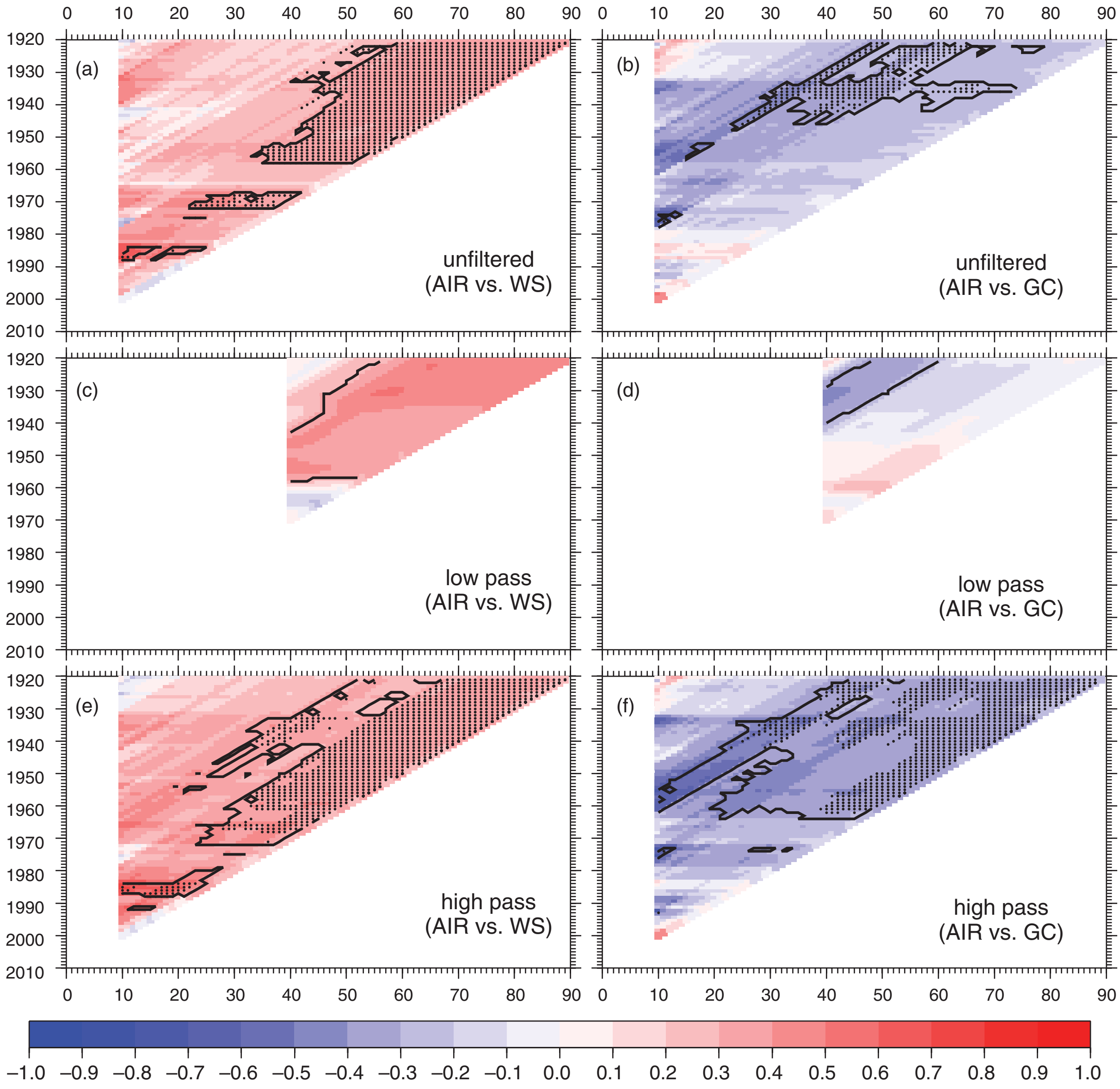

Figure 12. Correlation coefficients between the July–September indices of the All Indian Rainfall Index and of the standardized rainfall anomalies for West Sahel (left panels) and Guinea Coast (right panels), for all starting years (ordinate) and time sample sizes (abscissa). (a, b) Unfiltered component; (c, d) low-frequency component, i.e. longer than 8 years. Here, only window length of ≥40 years is displayed. (e, f) High-frequency component, i.e. shorter than 8 years. Contours (stippling) denote areas above the 95% significance level according to the F-test using standard degree of freedom (effective degree of freedom).

predictand, i.e. the standardized rainfall index for WS, CS, and GC. Unmatched predictors are indicated by '–' sign in Table 2. Thus, the following theoretical multi-linear models have been identified:

$$\mathrm{WS} = \alpha_0 + \alpha_1\mathrm{AMO} + \alpha_2\mathrm{N3.4} + \alpha_3\mathrm{ATL3} + \alpha_4\mathrm{IO} + \alpha_5\mathrm{EMS} \quad (1)$$

$$\mathrm{CS} = \beta_0 + \beta_1\mathrm{AMO} + \beta_2\mathrm{PDO} + \beta_3\mathrm{ATL3} + \beta_4\mathrm{IO} + \beta_5\mathrm{EMS} + \beta_6\mathrm{AIR} \quad (2)$$

$$\mathrm{GC} = \gamma_0 + \gamma_1\mathrm{AMO} + \gamma_2\mathrm{N3.4} + \gamma_3\mathrm{ATL3} + \gamma_4\mathrm{IO} \quad (3)$$

where α_0, β_0, γ_0 are the intercepts and α_1, α_2, α_3, α_4, α_5, β_1, β_2, β_3, β_4, β_5, β_6, γ_1, γ_2, γ_3, and γ_4 are the coefficients of the multi-linear regressions.

The correlation coefficients of the following multi-linear models are calculated using the adjusted coefficients of determination, which is a modification of the standard coefficient of determination that adjusts for the number of explanatory variables (predictors) in the model. The influence of the number of predictor variables is then taken into account and will not influence the computed correlation coefficients.

Figure 13 illustrates the multi-linear correlation coefficients for each multi-linear model and for all time periods. Only unfiltered data is considered here. Strongest

Table 2. Selection of adequate predictive variables for each predictand with the corresponding coefficient of regression including the intercept and using the longest available period, 1921–2009.

Predictands	WS	CS	GC
Predictors			
AMO	1.312	0.6488	−0.404
N3.4	−0.203	–	0.1230
PDO	–	−0.124	–
IO SSTs	−1.075	−0.763	−0.665
ATL3 SSTs	−0.525	−0.311	0.755
EMS SSTs	0.368	0.655	–
AIR	–	0.128	–
Intercept	33.426	12.176	−0.313

The '–' indicates unmatched predictors. The method of selection is described in Section 2.3.

multi-linear correlations between WS rainfall and the corresponding predictors (Figure 13(a)) are highlighted during two periods; in the earlier years starting from 1921 to 1955 and in recent years from 1980 onward. For the both two periods, the multi-linear regression model in Eq. 1 explains about 49–55% of the variation of WS rainfall. However, the PVE drops from 1960 to 1970 when compared to earlier and later years (Figure 13(a)). Then, the PVE of the WS rainfall explained by the selective predictive variables suggests a good quality of the prediction of WS rainfall. Similar patterns, as for the WS are observed for the CS (Figure 13(b)). The multi-linear correlation coefficients are also higher in the earlier years and in recent years starting in this case from 1975 onward. The values of the multi-linear correlation for these two previous periods are respectively on the range of 0.6–0.7 and 0.7–0.8. The drop in multi-linear correlation for the CS rainfall after 1960 and until about 1975 is shorter in time and less pronounced. For WS as for CS, the recent 35 years are characterized by very high correlations of up to 0.8. Figure 13(c) shows lower correlation coefficients in all time samples compared to previous cases for the GC indicating that the selected predictors are less suitable for describing the GC rainfall.

For interpreting the value or the nature of the multi-linear correlation, the relative importance contribution of each predictor for the description (or the prediction) of the corresponding predictand is examined. Figure 14 represents the relative importance of the predictors based on the PMVD criterion (cf. Section 2.3) for the full time series (1921–2009). The WS rainfall is driven mostly by IO SSTs with a contribution of 40% to the PVE (i.e. the coefficient of determination). AMO and N3.4 also contribute to the variability of the WS rainfall with 22 and 18%, respectively (Figure 14(a)). These three predictands should explain the high multi-linear correlation coefficients observed in Figure 13(a). More predictors are needed to characterize the CS rainfall variability; the ocean forcing (EMS, IO, and ATL3 SSTs) provides the strongest contributions, adding up to about 73% and which are dominated by the EMS SSTs (Figure 14b). The same pattern is seen for the rainfall of

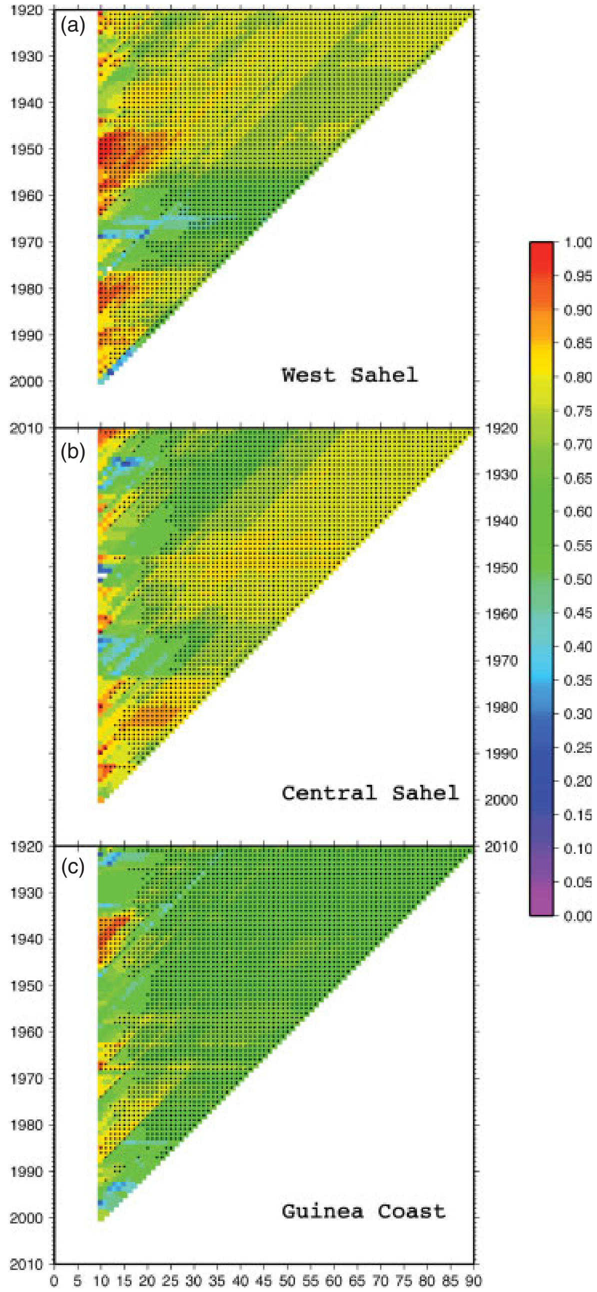

Figure 13. Multi-linear correlation coefficients between each West African region rainfall index (a) WS, (b) CS, and (c) GC (predictands) and the selected indices of climate variability (predictive variables). Stippled areas denote exceedance of the 95% significant levels according to the F-test and the SDOF. For more details, see text.

the GC, where the combined ATL3/IO contribution for describing the rainfall is at about 80%, compared to 12% from AMO and 8% from N3.4 (Figure 14(c)). Contrary to the Sahel, the predictive capacity of the ATL3 for GC JJAS rainfall is outperforming all other predictands.

5. Discussions and conclusions

Using a homogeneous West African station rainfall data set and a variety of indices of climate variability for the period 1921–2009 in a simple (multi-) linear correlation

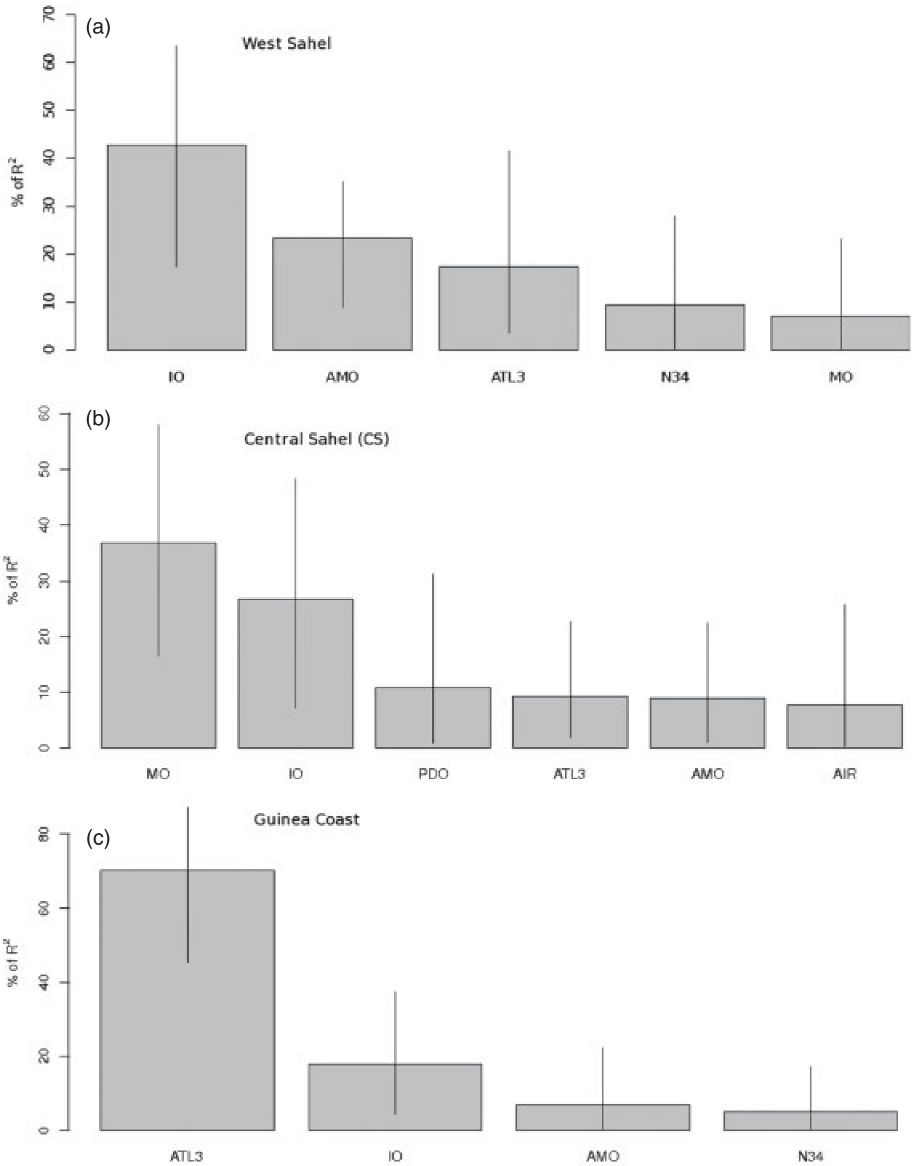

Figure 14. Relative importance with 95% bootstrap confidence intervals (according to coefficient of determination) of predictors for the description of rainfall of each WAM region. (a) WS, (b) CS, and (c) GC rainfall.

analyses approach, the stationarity of linear correlations over time for various time window lengths was assessed. West Africa was divided into three homogeneous rainfall regions and correlations were studied for unfiltered, low-pass, and high-pass filtered time series separating periodicities larger and smaller than 8 years. Lagged correlations have been tested, but except for ENSO indices, synchronous correlations were largest. The major findings are:

- The AMO and AMM show a positive linear correlation to unfiltered Sahel rainfall with a PVE of about 10–25%. The correlation largely stems from periods longer than 8 years for the AMO, whereas the AMM also exhibits a correlation on interannual time scales for WS rainfall, suggesting a closer physical relation between the AMM and WS rainfall when compared to the CS. The correlation between AMM and WS on decadal time scales is likely due to the excitement of decadal variability of AMM by AMO (Kossin and Vimont, 2007).
- A particularly robust and statistically significant correlation between ENSO indices (namely with N3.4 and ONI indices) and Sahel rainfall has been identified that mainly results from interannual fluctuation with a low PVE on the order of 10%. As the negative correlation increases in recent decades for N3.4, the positive correlation to SOI decreases. Thus N3.4 and ONI are better suited as WAM predictands than SOI. Correlations on decadal time scales may reflect ENSO-induced variability of the PDO (Newman *et al.*, 2003) that shows a significant negative correlation with Sahel rainfall.
- Evidence of strong connections between WAM rainfall and SSTs of adjacent oceans has been shown. From starting years between 1921 and 1960, the IO SSTs

explain about 16–36% of the variation of rainfall in the Sahel. These correlations are from decadal time scales, but weakened recently. Whether this weakening points to a recent more dominant influence of the AMO (Mohino *et al.*, 2011a) is plausible, but cannot be inferred from the present analyses due to the insufficient time series length.

- The EMS SSTs only impact significantly on rainfall in the CS and for long-term time samples starting between 1921 and 1925. In the most recent decades, a recovery has been observed with a PVE of about 36–47%. The signal is more established on the interannual time scale than on decadal time scales.
- The ATL3 SSTs have a positive strong and robust influence on GC rainfall at the interannual time scale. The relationship is significant and well established over the entire investigation period for all windows lengths, with PVE sometimes over 50%. For WS, the influence of the ATL3 SSTs presents two patterns. Negative correlations driven by the interannual band are found for starting years before the 1970s, and for the most recent years (i.e. decades after 1980) the correlations coefficients are significantly positive.
- The AIR is positively (negatively) linked to the WS (GC) rainfall variation for starting years between 1921 and 1970 and for window time lengths of 40–89 years. This weak relation is established on interannual time scales, has always been weak, and has deteriorated in recent decades, suggesting a change in physical mechanisms responsible for this correlation.
- Multi-linear regression analyses show that WAM rainfall can be predicted with rather good skill when simultaneous (June–September) combinations of adequate indices of climate variability (i.e. teleconnections indices) are used. The IO SST is the best predictor based on the entire investigation period for the WS. For the CS, it is the EMS SSTs, for the GC overwhelmingly the ATL3 SSTs.

One pertinent finding is that the AMM versus WS rainfall relation also at times exhibited significant correlations on interannual times scales, though this relation was absent between 1970 and 1990. The AMM is considered to be a physical mode of Atlantic SSTs and near-surface wind fluctuations in the tropical Atlantic. It has two activity poles straddling the equator. Though it has its maximum amplitude in boreal spring, it is known to be associated with Atlantic hurricane activity in boreal summer and early fall (Kossin and Vimont, 2007). The latter authors found a better correlation between the AMM and Atlantic hurricane activity when compared to the AMO. As AMM is known to show covariability with AMO on decadal time scales, the statistical analyses here suggests that the AMM is more closely related to WS rainfall than AMO on all considered time scales.

The presented work hints at several non-stationarities between the climate state indices and West African rainfall over a near-century long observation period. However, for the entire investigation period and a 31-year window, only the running correlation between WS Sahel rainfall and both, ATL3 and AMO, is significantly non-stationary from a statistical point of view. For the same time window length, the non-stationary behaviour of the ENSO indices and Sahel rainfall does not pass the significance test. However, there are physical arguments from modelling studies explaining a stronger ENSO influence in the recent period (e.g. Janicot *et al.*, 2001) which was shown in this study to be better reflected by using N3.4 or ONI as a predictor variable. The relation between ATL3 and WS changed from significantly negative to positive that could be explained by the less frequent and/or weaker occurrence of Sahel dipole years after 1970 – this has indeed been noted by Mohino *et al.* (2011a) who attributed this to the recent link between an Atlantic and Pacific Niño events, the latter suppressing the Sahel rainfall enhancement in Atlantic warm years (cf. Rodríguez-Fonseca *et al.*, 2011; Losada *et al.*, 2012).

The discussed non-stationarities cast doubt on the suitability of using multi-linear regression techniques for seasonal prediction of WAM rainfall. The only exception is the high and sustained predictive skill of ATL3 SSTs for the GC rainfall, with little additional skill from other predictors like ENSO indices. This is consistent with earlier studies (e.g. Fontaine *et al.*, 1998; Paeth and Hense, 2006). For the Sahel, statistical regression techniques for seasonal forecasting must consider different 'teleconnection regimes' for which the weighting of the predictors changes. The changing role of SST anomalies in the equatorial eastern Atlantic Ocean for WS rainfall is one proven example. Another example may be the recently dominating AMO influence on Sahel rainfall that weakened the IO SST influence. The latter speculation is an avenue of future research.

Acknowledgements

The first author was supported by the Alexander von Humboldt Foundation through a Georg Forster Research Fellowship. The second author acknowledges support by the QWeCI (EU Grant 243964) and most recently by the MIKLIP VESPA (BMBF Grant 01 LP 1110 B) projects to update the West African rainfall time series. The authors wish to thank Robert Schuster for fruitful discussion regarding the significance test of running correlations. They also thank the anonymous reviewer for his/her comments that helped to greatly improve the manuscript.

References

Akaike H. 1974. A new look at the statistical model identification. *IEEE Trans. Autom. Control* **19**: 716–723, DOI: 10.1109/TAC.1974.1100705.

Bader J, Latif M. 2003. The impact of decadal-scale Indian Ocean sea surface temperature anomalies on Sahelian rainfall and the North Atlantic Oscillation. *Geophys. Res. Lett.* **30**: 1–4, DOI: 10.1029/2003GL018426.

Biasutti M, Held IM, Sobel AH, Giannini A. 2008. SST forcings and Sahel rainfall variability in simulations of the twentieth and twenty-first centuries. *J. Clim.* **21**: 3471–3486, DOI: 10.1175/2007JCLI1896.1.

Butterworth S. 1930. On the theory of filter amplifiers. *Wireless Engineer* **7**: 536–541.

Chiang JCH, Vimont DJ. 2004. Analogous Pacific and Atlantic Meridional Modes of tropical atmosphere–ocean variability. *J. Clim.* **17**: 4143, DOI: 10.1175/JCLI4953.1.

Efroymson MA. 1960. Multiple regression analysis. In *Mathematical Methods for Digital Computers*, Ralston A, Wilf HS (eds). Wiley: New York, NY; 191–203.

Enfield DB, Mestas-Nuñez AM, Trimble PJ. 2001. The Atlantic Multidecadal Oscillation and its relation to rainfall and river flows in the continental U.S. *Geophys. Res. Lett.* **28**: 2077, DOI: 10.1029/2000GL012745.

Feldman B. 2005. *Relative Importance and Value*. http://www.prismanalytics.com/docs/RelativeImportance.pdf.

Fink A, Speth P. 1997. Some potential forcing mechanisms of the year-to-year variability of the tropical convection and its intraseasonal (25–70-day) variability. *Int. J. Climatol.* **17**: 1513–1534.

Fink AH, Schrage JM, Kotthaus S. 2010. On the potential causes of the nonstationary correlations between West African precipitation and Atlantic hurricane activity. *J. Clim.* **23**: 5437–5456, DOI: 10.1175/2010JCLI3356.1.

Folland C, Palmer T, Parker DE. 1986. Sahel rainfall and worldwide sea temperatures, 1901–85. *Nature* **320**: 602–607.

Fontaine B, Trzaska S, Janicot S. 1998. Evolution of the relationship between near global and Atlantic SST modes and the rainy season in West Africa: statistical analyses and sensitivity experiments. *Clim. Dyn.* **14**: 353–368, DOI: 10.1007/s003820050228.

Fontaine B, Garcia-Serrano J, Roucou P, Rodriguez-Fonseca B, Losada T, Chauvin F, Gervois S, Sivarajan S, Ruti P, Janicot S. 2009. Impacts of warm and cold situations in the Mediterranean basins on the West African monsoon: observed connection patterns (1979–2006) and climate simulations. *Clim. Dyn.* **35**: 95–114, DOI: 10.1007/s00382-009-0599-3.

Giannini A, Saravanan R, Chang P. 2003. Oceanic forcing of Sahel rainfall on interannual to interdecadal time scales. *Science* **302**: 1027–1030, DOI: 10.1126/science.1089357.

Grömping U. 2006. Relative importance for linear regression in R: the package relaimpo. *J. Stat. Softw.* **17**: 1–27.

Hagos SM, Cook KH. 2008. Ocean warming and late-twentieth-century Sahel drought and recovery. *J. Clim.* **21**: 3797–3814, DOI: 10.1175/2008JCLI2055.1.

Hoerling M, Hurrell J, Eischeid J, Phillips A. 2006. Detection and attribution of twentieth-century northern and southern African rainfall change. *J. Clim.* **19**: 3989–4008, DOI: 10.1175/JCLI3842.1.

Janicot S. 1992. Spatiotemporal variability of West African rainfall. Part II: associated surface and airmass characteristics. *J. Clim.* **5**: 499–511.

Janicot S, Moron V, Fontaine B. 1996. Sahel droughts and ENSO dynamics. *Geophys. Res. Lett.* **23**: 515, DOI: 10.1029/96GL00246.

Janicot S, Trzaska S, Poccard I. 2001. Summer Sahel-ENSO teleconnection and decadal time scale SST variations. *Clim. Dyn.* **18**: 303–320, DOI: 10.1007/s003820100172.

Kerr RA. 2000. A North Atlantic pacemaker for centuries. *Science* **288**: 1984–1985.

Kossin JP, Vimont DJ. 2007. A more general framework for understanding Atlantic hurricane variability and trends. *Bul. Amer. Meteor. Soc.* **88**: 1767–1781.

Kucharski F, Bracco A, Yoo JH, Tompkins AM, Feudale L, Ruti P, Dell'Aquila A. 2009. A Gill–Matsuno-type mechanism explains the tropical Atlantic influence on African and Indian monsoon rainfall. *Q. J. R. Meteorol. Soc.* **135**: 569–579, DOI: 10.1002/qj.406.

Losada T, Rodriguez-Fonseca B, Janicot S, Gervois S, Chauvin F, Ruti P. 2010. A multimodel approach to the Atlantic equatorial mode: impact on the West African monsoon. *Clim. Dyn.* **35**: 29–43, DOI: 10.1007/s00382-009-0625-5.

Losada T, Rodriguez-Fonseca B, Janicot S, Gervois S, Chauvin F, Ruti P. 2012. A multimodel approach to the Atlantic equatorial mode: Impact on the West African monsoon. *Geophys. Res. Lett.* **39**: L12705, DOI: 10.1029/2012GL052423.

Mohino E, Janicot S, Bader J. 2011a. Sahel rainfall and decadal to multi-decadal sea surface temperature variability. *Clim. Dyn.* , DOI: 10.1007/s00382-010-0867-2.

Mohino E, Rodríguez-Fonseca B, Losada T, Gervois S, Janicot S, Bader J, Ruti P, Chauvin F. 2011b. Changes in the interannual SST-forced signals on West African rainfall. AGCM intercomparison. *Clim. Dyn.* , DOI: 10.1007/s00382-011-1093-2.

Newman M, Compo GP, Alexander MA. 2003. ENSO-Forced Variability of the Pacific Decadal Oscillation. *J. Clim.* **16**: 3853–3857.

Nicholson SE. 2008. The intensity, location and structure of the tropical rainbelt over west Africa as factors in interannual variability. *Int. J. Climatol.* **28**: 1775–1785, DOI: 10.1002/joc.1507.

Nicholson SE, Palao IM. 1993. A re-evaluation of rainfall variability in the Sahel. Part I. characteristics of rainfall fluctuations. *Int. J. Climatol.* **13**: 371–389, DOI: 10.1002/joc.3370130403.

Paeth H, Hense A. 2006. On the linear response of tropical African climate to SST changes deduced from regional climate model simulations. *Theor. Appl. Climatol.* **83**: 1–19.

Palmer T, Brankovic C, Viterbo P. 1992. Modeling interannual variations of summer monsoons. *J. Clim.* **5**: 399–417.

Raicich F, Pinardi N, Navarra A. 2003. Teleconnections between Indian monsoon and Sahel rainfall and the Mediterranean. *Int. J. Climatol.* **23**: 173–186, DOI: 10.1002/joc.862.

Rayner NA, Parker DE, Horton EB, Folland CK, Alexander LV, Rowell DP, Kent EC, Kaplan A. 2003. Global analyses of sea surface temperature, sea ice, and night marine air temperature since the late nineteenth century. *J. Geophys. Res.* **108**, DOI: 10.1029/2002JD002670.

Rodríguez-Fonseca B, Polo I, Garcia-Serrano J, Losada T, Mohino E, Mechoso CR, Kucharsky F. 2009. Are Atlantic Niños enhancing Pacific ENSO events in recent decades? *Geophys. Res. Lett.* **36**: L20705, DOI: 10.1029/2009GL040048.

Rodríguez-Fonseca B, Janicot S, Mohino E, Losada T, Bader J, Caminade C, Chauvin F, Fontaine B, Garcia-Serrano J, Gervois S, Joly M, Polo I, Ruti P, Roucou P, Voldoire A. 2011. Interannual and decadal SST-forced responses of the West African monsoon. *Atmos. Sci. Lett.* **12**: 67–74, DOI: 10.1002/asl.308.

Rowell DP. 2003. The impact of Mediterranean SSTs on the Sahelian rainfall season. *J. Clim.* **16**: 849–862.

Rodwell MJ, Hoskins BJ. 1996. Monsoons and the dynamics of deserts. *Q. J. R. Meteorol. Soc.* **122**: 1385–1404.

Rowell DP, Folland CK, Maskell K, Ward NM. 1995. Variability of summer rainfall over tropical north Africa (1906–92): observations and modelling. *Q. J. R. Meteorol. Soc.* **121**: 669–704, DOI: 10.1256/smsqj.52310.

Saji NH, Goswami BN, Vinayachandran PN, Yamagata T. 1999. A dipole mode in the tropical Indian Ocean. *Nature* **401**: 360–363, DOI: 10.1038/43854.

Sutton RT, Hodson DLR. 2005. Atlantic Ocean forcing of North American and European summer climate. *Science* **309**: 115–118.

Taubenheim J. 1969. *Statistische Auswertung geophysikalischer und meteorologischer Daten*. Akadem. Verlag: Leipzig, Germany (In German).

Trenberth KE. 1984. Signal versus Noise in the Southern-Oscillation. *Mon. Weather Rev.* **112**: 326–332.

Trenberth KE, Hurrell JW. 1994. Decadal atmosphere–ocean variations in the Pacific. *Clim. Dyn.* **9**: 303–319, DOI: 10.1007/BF00204745.

Trenberth KE, Stepaniak DP. 2001. Indices of El Nino evolution. *J. Clim.* **14**: 1697–1701.

Van Oldenborgh GJ, Burgers G. 2005. Searching for decadal variations in ENSO precipitation teleconnections. *Geophys. Res. Lett.* **32**: L15701, DOI: 10.1029/2005GL023110.

Ward MN. 1998. Diagnosis and short-lead time prediction of summer rainfall in tropical North Africa at interannual and multidecadal timescales. *J. Clim.* **11**: 3167–3191.

Zeng N, Neelin JD, Lau KM, Tucker CJ. 1999. Enhancement of interdecadal climate variability in the Sahel by Vegetation interaction. *Science* **286**: 1537–1540, DOI: 10.1126/science.286.5444.1537.

Zhang Y, Wallace JM, Battisti DS. 1997. ENSO-like interdecadal variability: 1900–93. *J. Clim.* **10**: 1004–1020.

